1 (2026) 100032

Contents lists available at ScienceDirect

Biomass Futures

journal homepage: www.sciencedirect.com/journal/biomass-futures

TiO_2 photocatalysed biodiesel production through simultaneous esterification and transesterification of waste cooking oil

Rosilene A. Welter [a,b,*], Harrson Santana [b], Jayson Wau [a,c], Osvaldir Pereira Taranto [b], Michael Oelgemöller [a,d]

[a] College of Science and Engineering, James Cook University, Townsville, Queensland, 4811, Australia
[b] School of Chemical Engineering, University of Campinas, 13083-852, Campinas, S.P, Brazil
[c] School of Applied Science, Papua New Guinea University of Technology, Unitech Lae Papua New Guinea, Lae, 411, Papua New Guinea
[d] Faculty of Chemistry and Biology Institution, Hochschule Fresenius gGmbH, University of Applied Sciences, Limburger Str. 2, 65510 Idstein, Germany

ARTICLE INFO

Keywords:
Biodiesel
Free fatty acid
Photocatalysis
Titanium dioxide
Waste cooking oil

ABSTRACT

In this study, we explore the feasibility of TiO_2 photocatalysis in converting high free fatty acid (FFA) waste cooking oil (WCO) to biodiesel using a one-step esterification-transesterification. This approach has potential to convert high-FFA feed stocks into biodiesel without any use of homogeneous catalysts under mild operational conditions, applying either UVA or natural sunlight. The highest overall yield (83%) was achieved in methanolic solution and under UVA irradiation. The greatest conversion of 89% was obtained from the FFA fraction in esterification, whereas that of transesterification from triglycerides was 81%. Thereby different reaction pathways were presented under photocatalytic conditions. With UVA replaced by natural sunlight, the conversion decreased to 32% as it should be considered on account of photon limitations. Using ethanol instead of methanol resulted in only 21% conversion, highlighting the structure-selectivity of alcohol reactivity to photo absorption. Kinetic data were established by five different models and apparent rate constants as well as activation energies were calculated. Thermodynamic parameters ($\Delta H = 92.58$ kJ/mol, $\Delta S = 0.29$ kJ/mol·K) indicated that the process is endothermic, entropy-driven process that becomes thermodynamically favourable above 45 °C, which explains the reduced conversion at lower temperatures. After 5 cycles of using, the catalytic activity remained at a conversion up to 59% owing mostly to the organic deposition and catalyst agglomeration. In conclusion, it can also be seen that TiO_2 photocatalysis has a significant potential for sustainable biodiesel production from high-FFA waste feedstocks and, with scope for further optimisation and scale-up using renewable irradiation sources.

Nomenclature

Symbol/ Variable	Description	Unit
A	Arrhenius pre-exponential factor (frequency factor)	varies with reaction order
A_F	Pre-exponential factor of the forward reaction	varies
A_B	Pre-exponential factor of the backward reaction	varies
AV	Acid value	mg KOH g^{-1}
C*i*	Concentration of species *i*	mol L^{-1}
C_{max}	Maximum combustion rate	$(dW/dt)_{max}$
C_{mean}	Mean combustion rate	$(dW/dt)_{mean}$
CWP	Criterion for external mass-transfer limitation (Carberry–Weisz parameter)	–
ΔE_a	Activation energy	kJ mol^{-1}

(*continued on next column*)

(*continued*)

Symbol/ Variable	Description	Unit
ΔT_v	Range of temperature of volatiles	°C
$E_{a,F}$	Activation energy of the forward reaction	kJ mol^{-1}
$E_{a,B}$	Activation energy of the backward reaction	kJ mol^{-1}
Eα	Effective activation energy determined by isoconversional method	kJ mol^{-1}
FAME	Fatty acid methyl esters (biodiesel)	–
FAEE	Fatty acid ethyl esters	–
FFA	Free fatty acids	wt%
h^+	Photogenerated hole in TiO_2 valence band	–
e^-	Photogenerated electron in TiO_2 conduction band	–

(*continued on next page*)

* Corresponding author. College of Science and Engineering, James Cook University, Townsville, Queensland, 4811, Australia.
E-mail addresses: rosilene.weltergabas@jcu.edu.au (R.A. Welter), michael.oelgemoeller1969@gmail.com (M. Oelgemöller).

https://doi.org/10.1016/j.bmf.2026.100032
Received 30 November 2025; Received in revised form 15 February 2026; Accepted 17 February 2026
Available online 20 February 2026
3051-4444/© 2026 The Author(s). Published by Elsevier Ltd. This is an open access article under the CC BY license (http://creativecommons.org/licenses/by/4.0/).

(*continued*)

Symbol/ Variable	Description	Unit
k_1	Forward kinetic rate constant	varies with model
k_{-1}	Backward kinetic rate constant	varies with model
K_{eq}	Equilibrium constant	–
K'_1	Adsorption equilibrium constant of reactant species	L mol^{-1}
K'_2	Adsorption equilibrium constant of product species	L mol^{-1}
L–H	Langmuir–Hinshelwood kinetic model	–
MeOH	Methanol	–
MR	Molar ratio of alcohol:WCO	-
$M_{alcohol}$	Molar mass of alcohol	g/mol
N	Reaction order	–
Ω	Weisz–Prater criterion for internal diffusion limitation	–
R	Universal gas constant	J mol^{-1} K^{-1}
R^2	Coefficient of determination	–
T	Absolute temperature	K
T_B	Burnout temperature	°C
T_{bl}	Boiling point temperature	°C
T_{fp}	Flash point temperature	°C
TGL	Triglycerides	–
T_i	Ignition temperature	°C
TiO_2	Titanium dioxide photocatalyst (P25)	–
WCO	Waste cooking oil	–
x	Conversion	–
ρ	Density	kg/L or g/mL
ΔG	Gibbs free energy change	kJ mol^{-1}
ΔG_1	Gibbs free energy from equilibrium constant	kJ mol^{-1}
ΔG_2	Gibbs free energy from enthalpy–entropy relation	kJ mol^{-1}
ΔH	Enthalpy change of reaction	kJ mol^{-1}
ΔS	Entropy change of reaction	kJ mol^{-1} K^{-1}
Θ_{WCO}	Surface coverage fraction of WCO-derived species	–
Θ_{FAME}	Surface coverage fraction of FAME	–

1. Introduction

Biodiesel is an eco-friendly alternative to petrofuels. It has been produced globally on a large and growing scale due to increasing worldwide demand. Usually, it is blended into petrodiesel (5–10%) to obtain cleaner burning diesel fuel as it generate fewer greenhouse gases than petrodiesel (86% less) [1], and it is free of aromatics or sulphur [2]. It is made from crude vegetable oils and currently over 70% of intended feedstock for biodiesel production comes from edible vegetable oils [3], which competes with the food sector. Non-edible oils, including *Jatropha curcas*, have been proposed; however, these require land to produce the raw material as well, which indirectly competes with the food sector. As a cheaper and more sustainable approach, waste-cooking oil (WCO), which holds significant disposal problems, has been considered as a promising feedstock and its application increased from 3% (2007) to 11% (2019) [3].

Biodiesel production occurs through processes such as pyrolysis, esterification, and transesterification - the most common one [2]. Nevertheless, for feedstocks with a high amount of free fatty acids (e.g., WCO), it would be necessary to pretreat the feedstock in order to eliminate FFAs or alternatively employ catalysts that simultaneously induce triglyceride transesterification and FFA esterification. However, how to most effectively combine esterification and transesterification related to high free fatty acid (FFA) feedstocks without the need for oil preprocessing or harsh reaction conditions is still a controversial issue despite abundant literature studies, even including in photocatalytic mode. There is no typical process employing strong homogeneous alkali as it acts only as a catalyst for transesterification, which may lead to saponificationin the presence of water. Strong homogeneous acids are an alternative. However, the use of strong acids has prolonged inconveniences, such as their corrosiveness and therefore handling supply complication, product purification requirements, poor catalyst recovery or large amounts of waste produced [4]. These problems could be solved by application of heterogeneous catalysts in simultaneous esterification/transesterification reactions at mild operating conditions. Recent researches emphasise that high-FFA lipid feedstocks remain challenging as the process efficiency depends strongly on catalyst functionality and on integrating esterification and transesterification without complex pre-treatment and downstream separation steps [5,6].

Various heterogeneous catalysts have been tested, including photoactivated metal oxides. Titanium dioxide (TiO_2) is a widely known and one of the least expensive metal oxide semiconductors for photocatalysis. TiO_2 is non-toxic, chemically stable, and convenient in handling and recycling [7]. Moreover, photocatalysis applying TiO_2 has been considered as a promising pathway in diverse degradation and synthesis reactions [8–13]. For instance, the photoesterification of oleic acid achieved 96% conversion via TiO_2 mediated photocatalysis [13], and canola oil yielded 73% conversion via phototransesterification under similar experimental conditions. Khaligh et al. (2021) reached a 91% conversion of waste-cooking olive oil employing TiO_2 nanotubes as photocatalyst [14]. Khan et al. (2021) obtained an 89% WCO conversion by transesterification with a TiO_2-based composite with graphitic carbon nitride as catalyst. Even though, the WCO required a pretreatment with sulphuric acid to initiate FFA esterification [15]. Although these investigations illustrate the potential of TiO_2-UVA irraditaion, they vary significantly in feedstock formulations, catalyst designs, alcohol-to-oil ratios and input energy [16,17].

Moreover, the studies usually highlight that most photocatalytic and heterogeneous systems are still evaluated from a yield-oriented perspective, with limited integration of statistically discriminative kinetic modelling and experimentally supported thermodynamic analysis under photocatalytic regimes [18–20]. In particular, adsorption-controlled surface phenomena, reversibility constraints, and temperature-dependent feasibility are rarely assessed in a unified kinetic–thermodynamic framework, especially for high-FFA feedstocks such as waste cooking oil. Also, while comparatively fewer works integrate conversion outcomes with rigorous kinetic model discrimination and temperature-dependent thermodynamic interpretation to explain reversibility/spontaneity trends in a high-FFA feedstock under photocatalysis [21,22]. This limitation is significant because, without thermodynamic interpretation, temperature-dependent conversion trends cannot be reliably rationalized, hindering process optimisation, scale-up and reactor design. Therefore, a key gap remains in linking photocatalytic "simultaneous esterification/transesterification" performance to (i) a consistent kinetic framework (including forward/backward contributions) and (ii) thermodynamic parameters that rationalise temperature effects and feasibility. The absence of this combined analysis in the available literature not only puts a brake on mechanistic understanding but also makes it often impossible to compare among different catalytic systems or assess rigorously the scalability and operational windows [18,23]. By integrating experimental conversion data with detailed kinetic modelling and thermodynamic approach, the present work goes beyond simple performance reporting to provide a physicochemical basis for temperature effects, observed irreversibility, and pathway selectivity on high-FFA feedstocks in TiO_2 photocatalysis.

Accordingly, the present work aimed to provide an efficient methodology for biodiesel production from WCO involving simultaneous esterification and transesterification reactions based on experimental data acquisition, reaction mechanism proposal, kinetic and thermodynamic analyses establishment, physicochemical properties of reagents, products and catalyst calculation. The specific aims of this study were streamlined to: (i) ascertain the feasibility of a TiO_2 photocatalyst in environment-friendly simultaneous esterification and transesterification

of a real high-FFA WCO feedstock; (ii) elucidate a unifying kinetic/thermodynamic model correlating temperature-dependent efficacy; and (iii) examine both catalyst stability/reusability under photocatalytic operation. As a result, the key contributions of this work are: (i) a mechanistic explanation that connects photocatalytic conversion to kinetical model discrimination; and (ii) a justification for low conversion at low temperatures and feasibility at high temperatures due to experimental and thermodynamic properties iii) an evaluation of organic fouling on the catalyst surface caused by deactivated active sites due to the adsorption of organic species in higher-FFA systems. The distinctive aspect of this work is using the photocatalytic conversion data and multi-model kinetic analysis combined with thermodynamic to explain process behaviour: including temperature effects on feasibility for a real high-FFA WCO feedstock under UVA irradiation and natural sunlight.

2. Methodology

2.1. Materials

The reagents and solvents were obtained from the following suppliers: WCO (local restaurant, Townsville, Queensland, Australia), acetone (AR, 99.5%, Chemsupply), anhydrous sodium sulfate (Na_2SO_4, Univar), chloroform-D (99.8 atom % D, $CDCl_3$, Aldrich), dichloromethane (DCM, AR, 99.5%, Univar), diethyl ether (AR, 99.5%, Univar), ethanol (AR, 99.5%, Univar), ethyl acetate (AR, 99.5%, Univar), potassium hydroxide pellets (KOH, Univar), methanol (HPLC grade, Fisher Chemical), sodium bicarbonate ($NaHCO_3$, Univar), sulphuric acid (AR, Univar), TiO_2 (P25: Aeroxide®, Evonik), and 0.02 N potassium hydroxide in aqueous solution (aqueous KOH, ±0.5%, Ace Chemical Company), 1-oleoyl-rac-glycerol (Standard solution, Sigma), dioleoylglycerol (Standard solution, Sigma), 1,3-diolein (Standard solution, Sigma), Lipid Standard, Mono-, Di-, & Triglyceride Mix (Standard solution, Sigma), FAME mix (Standard solution, Supelco).

2.2. Simultaneous WCO esterification and transesterification

Fatty acid alkyl esters (biodiesel) production was studied via three reaction routes, namely acid-catalysed, UVA/TiO_2-photocatalysis and solar TiO_2-photocatalysis. The acid catalysis (Section 2.2.1) is the most typical thermal process that was presented in contrast with the photocatalysis (Section 2.2.2). For the two methods studied, two different alcohols were used: methanol for the production of fatty acid methyl esters and ethanol for the production of fatty acid ethyl esters (FAEEs).

2.2.1. Acid catalysed process

Simultaneous esterification and transesterification were conducted using sulphuric acid (H_2SO_4). This conventional method was chosen to provide a reference biodiesel that could be compared with the product obtained from TiO_2-photocatalysis. This reference system was not intended for kinetic or mechanistic comparison, but rather to provide a practical baseline for evaluating differences between conventional homogeneous catalysis and TiO_2-based photocatalysis biodiesel. The reactions were carried out in a round-bottom flask (500 mL) containing anhydrous alcohol (150 mL, methanol or ethanol), concentrated H_2SO_4 (1.5 g), and WCO (15 g), with vigorous mixing (magnetic stirrer, 500 rpm). The temperature was kept constant at 60 °C for 5 h. After this period, stirring was continued for 24 h at room temperature. The product was purified using the following steps: (1) 600 mL of water was added; (2) the mixture was rotary evaporated (40 °C, 170 mbar for 60 min, 72 mbar for 60 min, and 30 mbar for 60 min); (3) 150 mL of ethyl acetate was added; (4) the mixture was mixed gently; (5) phase separation was achieved in a separatory funnel after 1 h (steps 3 to 5 were conducted three consecutive times); (6) 150 mL of a diluted $NaHCO_3$ solution was added; (7) the mixture was mixed gently; (8) after 1 h of resting, phase separation was performed in a separatory funnel; (9) 150 mL of a saturated aqueous NaCl solution were added; (10) the mixture was mixed gently; (11) phase separation was conducted in a separatory funnel after resting for 1 h; (12) the organic layer was separated, and dried over anhydrous Na_2SO_4 for approximately 5 min; (13) the liquid fraction was filtered through a syringe filter (Hydraflon 0.22 μm, 35 mm); (14) the mixture was rotary evaporated at 40 °C to remove any volatiles (170 mbar for 30 min, 72 mbar for 30 min, and 30 mbar for 60 min); and (15) the samples were stored in glass vials at room temperature for further characterisation.

2.2.2. TiO_2-photocatalysed process

The protocol applied to the synthesis of biodiesel from WCO and alcohols by photoactivated TiO_2 was developed previously for oleic acid esterification [13] by an optimisation study (RSM-CCRD); where different operational parameters were evaluated (pre-treatment, reaction operational conditions (catalyst loading, reactants molar ratio, temperature), product purification, and catalyst reuse). Afterwards, the optimal conditions were successfully aplied to canola oil transesterification []. The protocol involved four stages: (1) catalyst pretreatment (Section 2.2.2.1); (2) photoirradiated reaction by UVA (Section 2.2.2.2) or sunlight (Section 2.2.2.3); (3) organic product purification (Section 2.2.2.4), and (4) catalyst analysis (Section 2.3). Moreover, blank tests were ran as described in Section 2.2.2.5.

2.2.2.1. Pre-treatment. Firstly, the pretreatment step comprised a previous mix of TiO_2 with the respective alcohol for 30 min before adding the oil and irradiation. It promotes catalyst wetting, minimises initial adsorption competition between reactants, and ensures homogeneous dispersion and effective contact between the alcohol, and TiO_2 surface prior to light irradiation, thereby improving reproducibility and reducing transient mass-transfer limitations at the beginning of the reaction.

2.2.2.2. TiO_2-UVA photoirradiated reaction. In the second step, the pretreated TiO_2-alcohol mixture and WCO were loaded into a jacketed two-necked round-bottom flask vessel (500 mL capacity) manufactured from Pyrex glass (cut-off wavelength ≤290 nm; Supplementary Material - Figure S1) under mixing (magnetic stirring, 500 rpm). Irradiation was carried out in a Rayonet photochemcial chamber reactor (RPR-200, Southern New England Ultraviolet Company) equipped with fluorescent tubes (Ushio, 16 F8T5/BL, 8W Black Light UVA T-5 G5 Base). The system (light and water bath) was turned on 30 min prior to starting the reaction. Operational conditions: 20% w/w_{wco} of TiO_2, 1 WCO mol:55 MeOH mol, total volume of reaction medium: 100 mL, and temperatures of 25–65 °C. Methanol evaporation was minimised by the use of a closed batch reactor equipped with a cooling finger and temperature-controlled water bath. No measurable mass loss was observed over the reaction period. Furthermore, the large excess of methanol ensured that minor evaporation effects did not affect reaction stoichiometry or kinetic interpretation.

TiO_2 loading of 20% w/w relative to WCO was selected based on prior optimisation studies conducted under analogous TiO_2-photocatalytic conditions, which demonstrated that lower catalyst loadings resulted in reduced conversion due to insufficient illuminated surface area and limited reactant–catalyst contact in biphasic systems. In slurry photocatalytic reactors, higher catalyst concentrations are often required to compensate for light scattering, partial photon shielding, and mass-transfer limitations associated with immiscible oil–alcohol mixtures. The selected catalyst loading represents a compromise between maximising the availability of photoactive sites and avoiding excessive light attenuation or aggregation effects.

A high methanol-to-oil molar ratio (1:55) was employed to overcome both thermodynamic and physicochemical limitations associated with esterification and transesterification of high-FFA feedstocks. Thermochemical studies have demonstrated that fatty acid esterification is an endothermic process and is not thermodynamically spontaneous at

moderate temperatures, requiring excess alcohol to shift the equilibrium towards ester formation by increasing the entropy contribution to the Gibbs free energy. In addition, excess methanol improves miscibility in the initially biphasic WCO–alcohol system, enhances phase homogeneity, and increases effective interfacial contact between reactants and the TiO_2 photocatalyst surface, thereby mitigating mass-transfer limitations under photocatalytic conditions [24].

The kinetic data samples (<3 mL each) were withdrawn at set reaction times (15, 30, 45, 60, 120, 180, and 240 min). Sampling times were deliberately selected to capture both the initial reaction regime (15–60 min), where rapid conversion occurs, and the slower approach to equilibrium (120–240 min), following the same kinetic protocol previously validated for TiO_2-photocatalysed esterification systems. This sampling strategy is consistent with previously reported photocatalytic esterification studies using TiO_2 under similar biphasic conditions. The reactions were conducted for 240 min, assuming that equilibrium was reached as no substantial variations were observed between 180 and 240 min under identical operating conditions, corroborating previous by authors who applied the same protocol [13].

All experiments conducted under the optimised operating conditions (65 °C) were performed in triplicate, and the reported conversion values represent the mean ± standard deviation. These conditions were selected as the reference case for kinetic modelling and thermodynamic analysis. Experiments performed at lower temperatures, under sunlight irradiation, or using ethanol instead of methanol were conducted as screening runs to establish comparative trends and temperature dependence, and were not subjected to full statistical replication.

The reaction medium was maintained under vigorous magnetic stirring, and the excess methanol ensured effective pseudo-homogeneous behaviour, minimising phase separation during irradiation and external mass-transfer limitations. Blank experiments (described ahead) performed without stirring resulted in a significant decrease in conversion, as further discussed in Section 3, and indicated that the applied stirring conditions were sufficient to eliminate mass-transfer limitations and that the reaction proceeded under kinetically controlled conditions. Alcohol evaporation was minimised by the use of a closed batch reactor equipped with a cooling finger and temperature-controlled water bath. The mass of the system was measured before and after running the reaction and no measurable mass loss was observed over the reaction period. Furthermore, the large excess of methanol ensured that minor evaporation effects did not affect reaction stoichiometry or kinetic interpretation. Fatty acid ethyl esters were obtained accordingly at 65 °C with ethanol instead of methanol.

2.2.2.3. TiO_2-sunlight photoirradiated reaction. An analogous process described for FAME above (Section 2.2.2.2) was performed at 65 °C, but applying sunlight instead of UVA light (Supplementary Material - Figure S2). A spherical stainless steel dish (inner diameter of 44 cm, focal length of 16.13 cm) was placed below the double-jacketed round-bottom reactor. The tests were run in the assembly allocated on the ground outside Science Place Building on the James Cook University campus in Townsville (latitude – 19°33′S, longitude 146°45′E, elevation 37.2 m above sea level) for 360 min, from 9:30 a.m. to 3:30 p.m. (January 7, 2022), the period with the strongest radiation, as shown in the Supplementary Material - Section S3, based on sunlight irradiation measurements obtained by ARPANSA [25].

To ensure further comparison between sunlight and UVA-lamp irradiation tests, the tests were conducted under the same operational conditions and using the same assembly. Although the bulk reaction temperature was maintained at 65 °C, only a limited fraction of natural sunlight lies within the UVA range (315–400 nm), the one required to photoactive the catalyst (TiO_2). As a result, the effective photon flux reaching the catalyst surface was substantially lower than under controlled UVA irradiation. In addition, light attenuation and scattering due to the slurry reactor and the steel dish further reduced the effective absorption path length, thereby limiting charge-carrier generation despite favourable thermal conditions.

2.2.2.4. Product purification. Firstly the reaction product was filtered through a syringe filter (Hydraflon 0.22 μm, 35 mm) and then rotary-evaporated at 40 °C to remove alcohol and water (170 mbar/15 min, 72 mbar/30 min, and 30 mbar/30 min), left to stand for 20 h to allow for glycerine separation and stored in glass vials at room temperature. The final samples (240 min) were characterised further (Section 2.4). The experiment at 65 °C was repeated three times, and the standard deviation was determined.

2.2.2.5. Blank tests. Five blank reactions were performed by keeping the operational conditions constant (65 °C, 1 WCO mol:55 MeOH mol, and 20% w/w_{WCO} of TiO_2). Blank 1 (absence of catalyst); Blank 2 (absence of light with the reaction vessel wrapped in aluminium foil); Blank 3 (absence of catalyst and light with the reaction vessel wrapped in aluminium foil); Blank 4 (absence of stirring); and Blank 5 (absence of catalyst pretreatment).

2.3. TiO_2 photocatalyst

2.3.1. Recovery and reuse

Before reusing the catalyst, the remaining reaction compounds (methanol, WCO, biodiesel, glycerides and water) adhered to the catalyst (0RP) were removed according to the following steps: (1) filtering the reaction mixture (Grade: MS 2185 mm, MicroScience), (2) washing with acetone by magnetic stirring (500 rpm), (3) settling for 24 h and decantation, (4) dried at 100 °C for 24 h. These steps are defined as the first phase of the recovery process (RP) and were performed three times (3 RP) to complete one reactivation cycle (1 C). The catalysts were placed into plastic vials and kept at room temperature. The recyclability of the regenerated and reused catalysts was studied based on the physicochemical properties (Section 2.3.1) and following photocatalytic reaction tests conducted up to 5 times (1C to 5C).

All the above-mentioned steps are relevant as they affect the catalyst purity, residual solvent content, bandgap, and the capacity to be reused in new reactions. Moreover, the weight of solids during all these steps was used to calculate the mass balance of the reaction medium, ensuring conversion reliability and determining the mass loss of both phases, liquid and solid. It is important to highlight that the error found in the mass balance was less than 1% due to the amount present in the catalyst, and it was not considered for further math. Although this recovery protocol is not optimised for industrial application, it was designed to ensure laboratory-scale reproducibility and controlled evaluation of catalyst deactivation. For future scale-up, a dedicated optimisation of the recovery step would be required to reduce complexity, processing time, and comprehend the economic approach. Nevertheless, the results demonstrate that catalyst recovery and reuse are feasible and that photocatalytic activity remains over multiple cycles, supporting the potential for further process development as shown in previous study [13].

2.3.2. Characterisation

TiO_2 was characterised prior to use (pure), after the photoreaction without further treatment (0RP), after the recovery process (1C, Section 2.3.1), and after use and recovery five times (5C).

Fourier transform infrared–attenuated total reflection (FTIR-ATR) spectroscopy: Functional group identifications were performed by FTIR-ATR coupled with an iD7 ATR accessory (Nicolet™ iS™ 5, room temperature, spectral range from 400 to 1000 cm^{-1}, ThermoFisher Scientific). Standard peaks are shown in the Supplementary Material (Section S4).

Thermogravimetric analysis and differential scanning calorimetry (5 °C/min, temperature range: room temperature – 600 °C, SDT650

equipment and Trios® software, TA Instruments) were carried out to determine the presence of organic material impregnated within the catalyst. The data were analysed using the Trios® software (TA Instruments), and OriginPro® 2022. The pure compounds and standards were analysed to be compared with the samples obtained from the different tests.

UV-Vis: UV-Vis spectra (spectral range of 200 – 1100 nm, UV-1800, room temperature, Shimadzu) were obtained using a TiO_2 suspension prepared by mixing (magnetic stirring) 10^{-3} mg/L TiO_2 in methanol for 4 h. The catalyst bandgap (E_g) was determined by applying the spectral data to the Tauc model, $(\alpha \cdot h\nu)^{1/\gamma} = B \cdot (h\nu - E_g)$ [26], which correlates the absorption coefficient (α), photon energy (hν), a constant (B) with a factor ($\gamma = 2$ for TiO_2 [27]), details regarding the symbols and units are given in the Nomenclature table).

2.4. Biodiesel characterisation

Gas chromatography wasused to evaluate the biodiesel composition according to the EN14103:2011 methodology [28] (7890A Agilent Gas Chormatograph, Injector: 7683B Agilent, HP-5INNOWax capillary column, 30 m × 0.25 mm, 0.25 μm film). Pure helium was used as a carrier gas (1 mL/min), with a 250 °C injector temperature, and 250 °C detector temperature; the temperature programme used was 60 °C/2 min, 10 °C/min to 200 °C, 5 °C/min to 240 °C, and holding at 240 °C/7 min. Compound identification was performed through standard retention times (Supplementary Material - Section S6).

^{1}H nuclear magnetic resonance spectroscopy was used to determine the conversions to FAME and FAEE (Bruker AscendTM 400 MHz Spectrometer, MestReNova® software, Version 6.0.2-5476, Mestrelab Research S.L., and OriginPro® 2022, Supplementary Material - Section S5). The conversion values were described as % biodiesel. The FAME amount ($\%\,FAME = 100\% \cdot 2 \cdot I_{ME}/3 \cdot I_{\alpha CH_2}$) was calculated by correlating the three methoxy protons (I_{Me}, approx. 3.6 ppm) with the two α-methylene protons of the oil ($I_{\alpha CH2}$, approx. 2.3 ppm), as described by Refs. [29,30]. The FAEE concentration was obtained similarly ($\%\,FAEE = 100\% \cdot (I_{GL+EE} - I_{GL})/I_{\alpha CH_2}$) by correlating the glyceride CH_2 (I_{GL}) and ethoxy (I_{EE}) proton areas (I_{GL+EE}, overlapping peaks at 4.10–4.20 ppm) with the α-methylene proton area of the oil ($I_{\alpha CH2}$, 2.3 ppm), as described by Ref. [31].

FTIR-ATR spectroscopy was used to analyse the oil and biodiesel qualitatively. Spectra deconvolution was delineated using OriginPro 2022® (Learning Edition, OriginLab Corporation). Peak deconvolution analysis was performed by PeakDeconvolution.opx from OriginLab®, with Straight Line as the baseline and Peak Resolution Enhancement Method: 2nd derivative Smooth Derivative Method:Quadratic Savitzky-Golay, 2nd order polynomial.

Acid values were determined by titration. The samples (0.05 g) were diluted in a diethyl ether/ethanol solution (2:1 v/v, 25 mL) with two drops of thymol blue indicator and titrated using 0.02 N standard aqueous KOH solution. The AV was determined by correlating the volume of the KOH solution used in the titration (S, mL), the volume of the KOH used in the blank titration (b, mL), the normality of KOH (N), and the sample mass (W, g): $AV = (S\text{-}b) \cdot N \cdot 56.1/W$.

TGA and DSC were carried out under N_2 and air (temperature range: room temperature – 600 °C, 5 °C/min) used to determine the boiling point ($dW/dT = 0$) and flash point (17.5% mass reduction), which indicates the lowest temperature at which the vapour could be ignited and the flame spread across the remaining liquid [32], ignition temperature (T_i) which refers to the temperature where the vapours have the capacity for autocombustion [33–35], burnout temperature (T_B, 95% mass reduction) [33,35], maximum combustion rate [C_{max}, $(dW/dT)_{max} = 0$] [35,36], and mean combustion rate [C_{mean}, $(dW/dT)_{mean}$ at 50% of mass reduction] [36].

2.5. Kinetic and thermodynamic properties

Simultaneous esterification/transesterification reactions were conducted until equilibrium conditions were reached (4 h) over the temperature range of 25 to 65 °C (Section 2.2.2). The kinetic experiments and sampling protocol were designed based on previously established TiO_2-photocatalysed esterification systems, ensuring consistency and reproducibility across studies [13,]. Internal and external mass transfer limitations were neglected, and it was assumed that the reaction were kinetically limited (Supplementary Material - Section S10). Five kinetic models were applied (Table 1). Four models considered a homogeneous system (F1B1, F1B2, F2B2, and F2B4, Equations (1)–(4), respectively), whereas the fifth (L–H, Equation (5)) considered the system as heterogeneous. involving a solid catalyst with homogeneous active sites and a system with complete miscibility among the reagents. Mathematical modelling was performed using the Matlab® software (algorithms applied: Lsqcurvefit, and ode45). The predicted data were statistically compared to the experimental data (by R^2, F-test, standard deviation, β, t-test, p-value). Moreover, through the kinetic rate constants (k_1 and k_{-1}), the equilibrium constant (K_{eq}) was determined. The activation energy (ΔE_a) and the frequency factor (A) were estimated using the Arrhenius model for both reactions (forward - Equation (6), and backward - Equation (7)). The effective activation energy (E_α, Equation (8)) was determined considering the isoconversional principles [37,38]. Subsequently, the thermodynamic properties were determined by the forward equations considering the model-based equilibrium constants calculated from kinetic data; and were not based on calorimetric measurments. The reaction enthalpy (ΔH_R) and entropy (ΔS) were estimated through linearisation of the Van't Hoff model (Equation (9)) and Gibbs free energy variation (ΔG) by two equations. First, correlating T and K_{eq} (Equation (10)); and second, correlating ΔH_R, T, and ΔS (Equation (11)), respectively.

$$\ln(k_1) = -\frac{\Delta Ea_F}{R \cdot T} + \ln(A_F) \quad \text{Equation 6}$$

$$\ln(k_{-1}) = -\frac{\Delta Ea_B}{R \cdot T} + \ln(A_B) \quad \text{Equation 7}$$

$$E\alpha = \frac{k_1 \cdot Ea_F + k_{-1} \cdot Ea_B}{k_1 + k_{-1}} \quad \text{Equation 8}$$

$$\ln(K_{eq}) = -\frac{\Delta H_R}{R \cdot T} + \frac{\Delta S}{R} \quad \text{Equation 9}$$

$$\Delta G_1 = -R \cdot T \cdot \ln(K_{eq}) \quad \text{Equation 10}$$

$$\Delta G_2 = \Delta H_R - T \cdot \Delta S \quad \text{Equation 11}$$

3. Results and discussion

3.1. WCO esterification/transesterification

The simultaneous esterification and transesterification of WCO were analysed considering the effects of temperature, catalyst reuse, TiO_2 presence, stirring, light and different alcohols and are shown in (Fig. 1). The highest efficiency was 83% (±1.24%, average of triplicate experiments, Fig. 1). It was achieved for WCO with methanol, under TiO_2 photocatalysis in 4 h (equilibrium), using the following conditions: UVA light, batch reactor, stirring at 500 rpm, 1 WCO:55 MeOH molar ratio, 20% w/w_{wco}, and T = 65 °C.

This catalyst loading was chosen from a prior systematic optimisation study performed by the authors in which different operational conditions were studied by response surface methodology (TiO_2 loadings from 1 to 30% w/w, molar ratio between 1:3 and 1:55, and temperature from 25 to 65 °C) [13]. In that study, 20% w/w TiO_2 afforded the highest conversion at all conditions studied, while increasing

Table 1
Kinetic models evaluated for simultaneous WCO and methanol esterification/transesterification photocatalysed by TiO_2.

Assumptions	Model Equation	
Homogeneous system		
F1B1 - F: first-order - B: first-order	$\frac{dx_{wco}}{dt} = k_{-1} \cdot (1 - x_{wco}) - k_1 \cdot x_{wco}$	Equation 1
F1B2 - F: pseudo first-order - B.: second-order	$\frac{dx_{TGL}}{dt} = k_{-1} \cdot (1 - x_{TGL}) - k_1 \cdot C_{TGL_0} \cdot x_{TGL}^2$	Equation 2
F2B2 - F: second-order - B: second-order	$\frac{dx_{wco}}{dt} = k_{-1} \cdot C_{wco_0} \cdot (1 - x_{wco})^2 - k_1 \cdot C_{wco_0} \cdot x_{wco}^2$	Equation 3
F2B4 - F: Second-order - B: fourth-order	$\frac{dx_{TGL}}{dt} = k_1 \cdot C_{TGL_0} \cdot (1 - x_{TGL})^2 - k_{-1} \cdot C_{TGL_0}^3 \cdot x_{TGL}^4$	Equation 4
Heterogeneous system		
L–H kinetic model[a] - F: first-order - B: first-order - FAME is bounding the catalyst capacity	$\frac{dx_{wco}}{dt} = k_{-1} \cdot \frac{K'_2 \cdot x_{wco}}{1 + K'_2 \cdot C_{wco_0} \cdot x_{wco}} - k_1 \cdot \frac{K'_1 \cdot (1 - x_{wco})}{1 + K'_1 \cdot C_{wco_0} \cdot (1 - x_{wco})}$	Equation 5

[a] details of the model development can be found in supplementary material - Section S9; F: Forward reaction; B: Backward reaction.

loadings caused a fall in activity due to light scattering and particle agglomeration effects. Based on these results, in this work, the photocatalytic route was tested for real waste cooking oil feedstocks where both esterification and transesterification reactions take place in a chemically and optically more complex system. Therefore, the catalyst loading applied in the present work reflects an optimal balance between illuminated active surface area and photon penetration in an optically dense reaction medium, rather than catalyst site saturation. Compared with other studies (Table 2), this result indicates that photocatalysis can be applied to biodiesel production using a feedstock with a high FFA content.

Evaluating the FFA content (Table 4), the initial feedstock had about 10.9% of FFA, while the product from TiO_2-UVA photoirradiated in the presence of methanol had only 1.2% and the product from acid reaction only 0.2%. The decrease indicates the esterification reaction in both cases, with an efficiency of 89% for TiO_2-UVA photoirradiated system. Considering this value and by the mass balance of the TiO_2-UVA photoirradiated, the transesterification route resulted in an efficiency slightly lower, about 81%. These values correspond to pathway-specific conversions and do not represent contradictory measurements of the same parameter. This difference highlights that esterification and transesterification do not proceed with identical kinetics or surface interactions under TiO_2 photocatalysis. Free fatty acids can directly interact with Lewis acidic Ti^{4+} surface sites through their carboxylate groups, whereas triglyceride transesterification involves bulkier molecules and multistep bond cleavage, making it more sensitive to surface coverage and reaction intermediates. However, due to the lower presence of FFA compared to the triglyceres, the focus of the chemical mechanism, mathematical modelling, and consequent parameters focus only on the transesterification process.

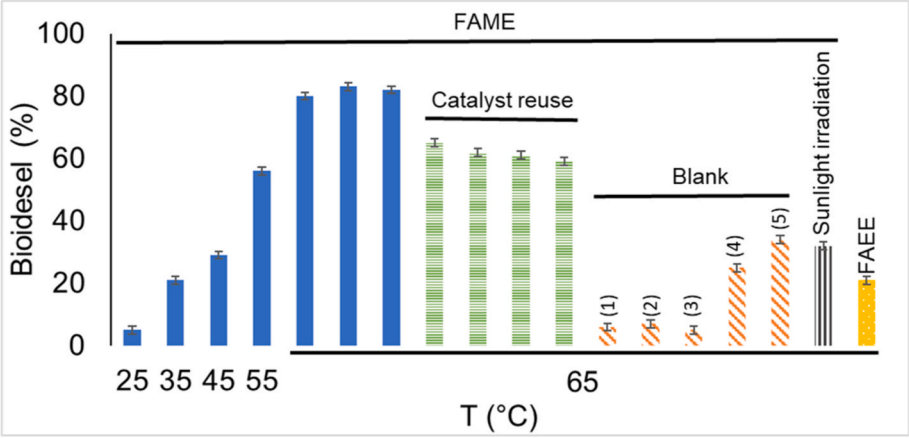


Fig. 1. Simultaneous WCO and alcohol esterification/transesterification was conducted to produce biodiesel by TiO_2-photocatalysis. Biodiesel (%) was obtained using ^1H NMR as described in Section 2.4. Regular runs: ■ WCO-Methanol, UVA light irradiation, 25–565 °C. Catalyst reuse: ▤ a total of 4 photoreactions were conducted subsequently with reused catalyst (2C–5C). Blank runs in the absence of: ▨ (1) TiO_2; (2) irradiation; (3) TiO_2 and irradiation; (4) stirring; (5) TiO_2 pretreatment. Others: ▥ Sunlight illumination; ■ WCO-Ethanol. Operational conditions (if applicable): 1 WCO:55 alcohol molar ratio and 20% TiO_2 (w/w_{wco}), UVA light irradiation. Standard deviation (σ) ±1.24 was determined in triplicate of the regular test (FAME) at 65 °C.

Table 2
Biodiesel produced from WCO catalysed by oxides.

Catalyst	% (w/w_{wco})	Alcohol	Molar ratio	T (°C)	Time (h)	FAME (%)	Ref.
CaO.ZnO	2	Methanol	10	70	60	95	[39]
CuO/ZnO + UVA	5	Ethanol	9	65	120	93	[40]
ZnO-La_2O_3	2	Methanol	[a]	200	3	96	[41]
TiO_2	4	Methanol	10	120	4	91	[42]
TiO_2/g-C_3N_4 + sunlight	2	Methanol	9	60	60	84	[15]
TiO_2/Graphene	1.5	Methanol	12	65	3	98	[30]
TiO_2-MgO	10	Methanol	30	160	6	92	[43]
TiO_2/$PrSO_3H$	1	Methanol	6	65	9	98	[40]
TiO_2 + sunlight	nanotubes	Methanol	8	60	4	91	[14]
TiO_2 + sunlight	20	Methanol	55	65	6	32	TS[c]
TiO_2 + UVA	20	Ethanol	55	65	4	21	TS[c]
TiO_2 + UVA	20	Methanol	55	65	4	82[b]	TS
Esterification						89	TS
Transesterification						81	TS

[a] 126 g of oil and 180g of methanol.
[b] 82% refers to the total conversion being 89% FFA esterification and 81% TGL transesterification.
[c] TS: this study.

Table 3
Oxide catalyst reuse for biodiesel production from WCO.

Catalyst	FAME (%)	# cycles	FAME (%)[a]	Decrease (%)[b]	Ref.
CuO/ZnO + UVA	93	6	80	13	[40]
SrO-ZnO/Al_2O_3	96	3	17	79	[44]
TiO_2/Graphene	98	3	79	19	[30]
TiO_2-MgO	92	5	81	11	[43]
TiO_2 + UVA	73	5	36	37	This study

[a] Conversion determined for the final cycle.
[b] Decrease between the first and last cycle.

Table 4
Characterisation of WCO and biodiesel obtained by acid catalysis and photocatalysis.

		WCO	FAME	
			TiO_2+UVA	Acid
FFA	(%)	10.9 (±0.5)	1.2 (±0.2)	0.2 (±0.1)
T_{bp}	(°C)	413	230	229
T_i	(°C)	365	183	181
T_{fp}	(°C)	377	190	188
T_B	(°C)	454	248	306
C_{max}	$(dW/dt)_{max}$	1.8	1.4	1.9
C_{mean}	$(dW/dt)_{mean}$	0.8	0.5	1.0

A reduction of 37% between the first and fifth cycles was observed. As shown in Table 3, other authors have also detected reductions in activity with solid catalysts and this has been linked to the changes in physicochemical properties of catalyst amount. The presence of organic species inside the catalyst is affecting its efficacy in this case, as discussed in details in Section 3.5.

The operational conditions obtained for UVA-irradiation that resulted in the highest efficiency (WCO + methanol, 4 h, batch reactor, stirring at 500 rpm, 1WCO:55MeOH molar ratio, 20% w/w_{wco}, and T = 65 °C) were applied for sunlight instead of UVA. TiO_2 is photoactivated by UVA light between 315 and 400 nm. Sunlight only has a small fraction and low UVA intensity [45], naturally resulting in reduced activation. As shown by the solar spectral distribution (Fig. S3), only a limited portion of the incident solar radiation meets the energetic requirement to overcome the TiO_2 bandgap (~3.2 eV). Although sunlight irradiation resulted in lower conversion, this behaviour reflects photonic rather than thermal limitations. TiO_2 activation depends on photons with energy equal to or greater than its bandgap, and the limited UVA fraction in natural sunlight reduces charge-carrier generation and increases recombination, thereby constraining photocatalytic efficiency despite favourable reaction temperatures. Nevertheless, a notable conversion was reached, indicating that the solar TiO_2-photocatalysed reaction is generally feasible. To achieve higher conversion, a larger exposure surface, a hybrid solar-lamp system, an optimised solar reactor design to concentrate the sunlight may be applied [46].

Optimum conditions (UVA light irradiation, 4 h, batch reactor, stirring at 500 rpm, 1WCO:55MeOH molar ratio, 20% w/w_{wco}, and T = 65 °C) were then applied usimg ethanol instead of methanol, and an efficiency of 38% was achieved. Other researchers also found a decline in stability with alternative solid catalysts [13, 49, 50]. Methanol is a stronger electron donor and its reactivity is higher than that of other alcohols [47,48]. While the miscibility of WCO and methanol is not as high as that of ethanol, both alcohols provided a homogeneous system at higher temperatures (65 °C) when mixed for mass transport. The better efficiency of methanol should have its origin not only from the stronger electron donation capability but also from the smaller molecular size, which results in a more efficient formation of surface alkoxides and interfacial reaction kinetics on TiO_2. This suggests that alcohol structure has an effect on photocatalytic reactivity, beyond the bulk phase miscibility effects. Mechanistically, such inhibition in the photocatalysis of ethanol can be rationalized by interfacial kinetic and thermodynamic control factors which become most important under photocatalytic conditions. Ethanol makes larger ethoxy intermediates on the TiO_2 surface than methanol and these combine to give rise to slower rates of surface alkoxide production (based upon CH_3CHO) as well as limited reactivity for adsorbed acyl species. It leads to inefficient utilization of photogenerated charge carriers and a high probability for electron–hole recombination.

Five blank runs were carried out under the optimum operational conditions to produce FAME. In the absence of TiO_2, UVA light or both were observed conversions lower than 10%, establishing both that irradiation and a proper photocatalyst are required. The low mixing intensity led to as low as a 25% conversion and resulted from inadequate mass transfer. Without pretreatment, the experimental run gave a conversion of 34% whereas with pretreatment it reached 83%. Without pretreatment, the catalyst pores also tended to be adsorbed by other reagents which led to deterioratiom in the capacity of absorbing light and hence in efficiency. The loss of catalytic activity was attributed to the 23% reduction from the first (1C) to fifth (5C) cycles, which was attributed to changes in catalyst nature as detailed in Section 3.5.

3.2. FAME characterisation

The initial feedstock (WCO) and the biodiesel produced were characterised as described in Table 4. The content of FFA was obtained initially by titration for WCO (10.9%), for FAME from acid catalysis (0.2%) and from photocatytic synthesis (1.2%). The FFA value determined in WCO is in accordance with the literature (5–20%) [47–49]. A second technique was applied (FTIR-ATR spectroscopy). In this case, as shown in Fig. 2, the value was obtained by the peak deconvolution of FTIR-ATR spectra (see Supplementary Material - Section S4). Nevertheless, only the crude WCO showed a good agreement between titration and FTIR-ATR peak deconvolution data. The comparability between the two techniques was lower for FAME analyses [FAME from photocatalysis: 1.5% (FTIR-ATR), 1.2% (Titration); FAME from acid catalysis: 1.1% (FTIR-ATR), 0.2% (titration)]. It can be explained as, at low residual FFA levels, FTIR-based quantification exhibits higher variability due to the weak intensity of acid carbonyl bands and their overlap with the dominant ester carbonyl absorption of FAME. Under these conditions, small variations in baseline correction and peak deconvolution can result in a relatively large uncertainty. FTIR analysis was therefore applied as a semi-quantitative technique to monitor relative trends, while titration was used as the reference method for absolute FFA determination. Titration proved to be the morst precise methodology with a low standard deviation after triplicate determination. For small peaks, FTIR-ATR spectral deconvolutions, on the other hand, were considerably influenced by noise in the spectrum. Notably, the major peak derived from FFA in the FAME spectrum drifted when its concentration was low.

A strong reduction in the FFA amount was anticipated for acid catalysis since esterification as well as transesterification proceeded under these conditions as verified by titration. Acid-catalysed transesterification (99% of conversion) was somewhat more effective than esterification (98% of conversion), and both reactions also occured during photocatalysis [13,14,42,43,52,41]. However, under photocatalysis esterification (89%) was slightly more efficient than transesterification (81%). Esterification was less energy-demanding than transesterification (and thus faster), hence a higher conversion was achieved. A decrease in the conversion of TGL compared that of FFA observed here may be attributed to multistep processes and steric hindrance of transesterification, which impose a stronger surface-kinetic and charge-transfer requirement than one-step esterification of FFA under photocatalysis. This difference reveals that, although esterification and transesterification occur, they actually evolve independently with separate surface interactions and kinetics pathways under TiO_2 photocatalysis, instead of a shared global transformation pathway. However, due to the higher amount of TGL compared to FFA in the feedstock, the focus of the parameter further determined was on the transesterification reaction. High conversions for an esterification (e.g., UVA-light irradiation of oleic acid with TiO_2) in a UVA system were also achieved, and results up to 98% conversion were observed [13], thus indicating that the substantial success with this approach was possible. It indicates that the method is less effective for transesterification than for esterification. This comparison is aligned with the observation that among free fatty acid esterification and triglyceride transesterification, molecular complexity and steric hindrance of triglycerides inhibit photocatalytic transesterification.

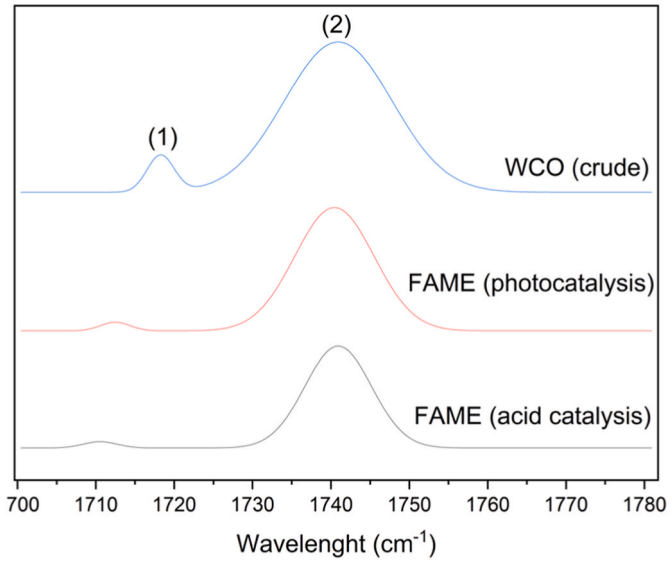


Fig. 2. Deconvoluted ATR–FTIR spectra of crude WCO and FAME obtained by simultaneous esterification and transesterification using acid catalysis and TiO_2/UVA photocatalysis. Spectral region: 1700–1780 cm^{-1}. Peak assignments: (1) ~1709 cm^{-1} corresponding to free fatty acids (C=O stretching of –COOH); (2) ~1740 cm^{-1} corresponding to ester carbonyl (C=O stretching of FAME). Deconvolution was applied to enhance peak discrimination in complex matrices; results are qualitative and intended for comparative analysis (see Supplementary Section S4) [13,50,51].

Thermoanalyses were conducted for raw WCO, FAME obtained by acid catalysis (Supplementary material – Section S6) and by photocatalysis (Table 4, Fig. 3, Supplementary material – Section S7). The boiling points (T_{bp}) of WCO and FAMEs were estimated to be 413 °C and 230 °C, respectively. The ignition temperatures (T_i) for biodiesel obtained from both methods were similar (183 and 181 °C, respectively) as were the flash point (T_{fp}, 190 and 188 °C, respectively). Between 100 and 150 °C (ΔT_v), no peaks were observed, indicating that are not volatile compounds were present. The similarity of these properties indicates that the FAMEs prepared from both catalysts are similar and highly thermally stable [35,53]. The Burnout temperature (TB), maximum combustion rate (C_{max}), and mean combustion rate (C_{mean}) of FAME obtained by photocatalysis were slightly less than those produced by acid catalysis. However, the trend of curve was found to be quite similar, which shows the FAME obtained by photocatalysis was thermically equivalent to that produced by acid catalysis (assumed as reference point) and the variation may be due to the presence of unconverted feedstock.

The biodiesel composition produced by thermal acid catalysis and photocatalysis was likewise determined by gas chromatography (Table 5). According to these results, under photocatalysis there is a tendency to convert more C18:1 (methyl oleate) and C19:1 (methyl nonadecanoate) than C18:2 (linoleic acid) which carries an additional double bond, and increases the energy required for the reaction [44]. The proposed mechanism is derived from the experimental trends observed in this work and is discussed within the context of established

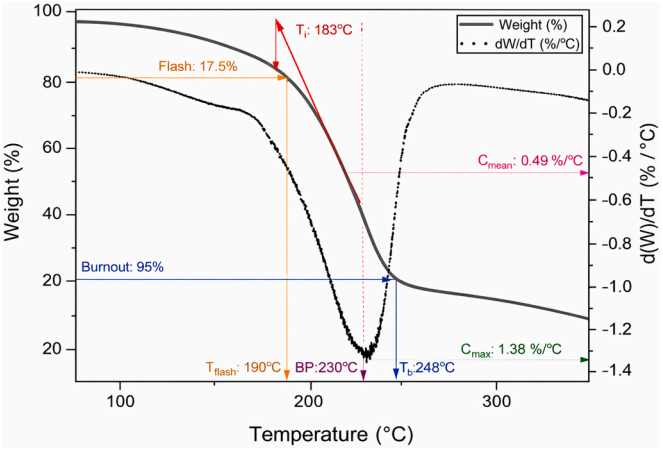


Fig. 3. TGA of biodiesel obtained by photocatalysis using WCO and methanol.

Table 5
Composition of biodiesel obtained by acid catalysis and photocatalysis[a].

		TiO_2+UVA	Acid
methyl hexanoate	C6:0	0.1	0.1
methyl decanoate	C10:0	0.1	0.1
methyl mmyristate	C14:0	0.5	0.5
methyl palmitate	C16:0	17.4	18.1
methyl palmitoleate	C16:1	0.4	0.4
methyl stearate	C18:0	2.9	3.0
methyl oleate	**C18:1**	**51.5**	**50.4**
methyl linoleate	**C18:2**	**21.0**	**25.0**
methyl linolenate	C18:3	1.4	1.1
methyl nonadecanoate	C19:0	3.6	0.5
methyl eicosonate	C20:1	0.5	0.7
methyl eicosadieonate	C20:2	0.7	0.0

[a] Obtained using GC (Supplementary Material - Section S6).

TiO_2 photocatalytic pathways rather than as a direct identification of individual reactive intermediates.

For example, the $\Delta H^{\circ}_{r,298K}$ for methyl oleate esterification (122 kJ/mol) is lower than that for methyl linoleate esterification (245 kJ/mol) [54]. In addition, computational studies on canola oil methyl esters showed that methyl nonadecanoate (C19:0) is slightly more reactive than methyl oleate (C18:1) as the C19:0 does not have the double bond present in the C18:1 sctructure [55]. Both studies indicate that the reaction kinetics are also driven by interaction between the TiO_2 surface and the π-electron interactions associated with multiple C=C bonds, which change due to the adsorption geometry and surface residence time. In particular, polyunsaturated chains (e.g., C18:2) contain bis-allylic positions that are more prone to H-abstraction and radical delocalisation, making them more susceptible to TiO_2-driven reactive oxygen species (•OH and $\bullet O_2^-$) pathways and competing photooxidation. Furthermore, radical intermediates derived from C18:2 can undergo delocalisation over conjugated double bonds, increasing susceptibility to competing photooxidation reactions and charge-carrier recombination. Additionally, the extra C=C bond can promote stronger/multi-point surface interactions (longer surface residence time), which can increase the probability of non-productive charge recombination and oxidative side reactions rather than productive ester formation. These effects reduce the fraction of photogenerated charges contributing to productive esterification, leading to lower apparent conversion compared to C18:1. Thus, the energy required increases with the number of double bonds, and subsequently conversions decrease, and the lower apparent conversion of C18:2 over the photocatalytic route is related to both (i) a more significant thermodynamic requirement and (ii) photoinduced surface/radical pathways that are more competitive for polyunsaturated species.

The presence of reaction intermediates, such as monoglycerides (MGL) and diacylglycerides (DGL) was found in trace levels as shown in Table 6. Although some authors detected their presence, they were only found in small concentrations at the beginning of the reaction [56,57]. It indicated that the intermediates formation and consumption occur rapidly. This behaviour is consistent with a quasi-steady-state regime, in which MGL and DGL are unstable structures, formed and consumed continuously. However, MGL and DGL are known to act as surfactants that can improve the miscibility between oil and alcohol [58]. Under photocatalytic conditions, such intermediates may act as transient in situ surfactants, temporarily enhancing interfacial contact and mass transfer between the immiscible phases while being rapidly converted as the reaction progresses.

Table 6
Composition of WCO, reaction intermediates and purified biodiesel at different conversion stages determined by GC-MS (%).

Sample	FAME	MAG	DAG	TAG	Glycerol
WCO (raw)	2.3	0.0	9.9	84.9	0.1
WCO + acid (1 h)	47.2	0.8	6.7	42.8	0.3
WCO + acid (complete)	96.1	0.6	0.6	0.0	0.5
WCO photocatalysis (crude)	91.1	0.4	1.8	4.6	0.6
WCO photocatalysis (after purification)	90.4	0.3	5.1	2.7	0.4

Values may not total 100% due to experimental uncertainty associated with GC–MS quantification and integration of minor components.

WCO conversions to biodiesel were furthermore analysed by ^{1}H NMR spectroscopy (Fig. 4, Supplementary Material - Section S5), and by FTIR-ATR spectroscopy (Fig. 5). In both analyses, the most important aspect is regarding the presence of impurities in the final product. Biodiesel obtained from acid catalysis required several purification steps including extraction using ethyl acetate (Section 2.2.1), which could not be quantitatively removed. The presence of residual solvent confirms the general difficulty of removing contaminants when using traditional processes. This highlights a well-known limitation of homogeneous acid catalysis, where downstream purification steps can introduce residual contaminants that are difficult to fully eliminate. In contrast, photocatalysis does not demand additional reagents or solvents for isolation or lengthy purification steps. It only requires filtration and decatnation, or even a centrifugation step, to physicallyseparate the phases. Thus, minimising waste production and avoiding additional contaminants in the biodiesel product. This difference reflects a fundamental distinction between homogeneous and heterogeneous catalytic pathways, in which photocatalysis allows reaction termination without chemical quenching or solvent-intensive separation. In this scenario, although the initial costs of photocatalysis are higher than the homogeneous pathway, the lower costs associatedwith purification and waste treatment offset the initial investiments involved in the TiO_2-UVA irradiatied system.

3.3. Proposed photocatalysis mechanism

The proposed reaction mechanism for the generation of biodiesel is shown in Fig. 6. It involves, two main pathways; esterification of FFA and transesterification of TGL. Firstly, the catalyst, TiO_2 in the presence of UVA light, releases enough energy to overcome its bandgap (3.2 eV,

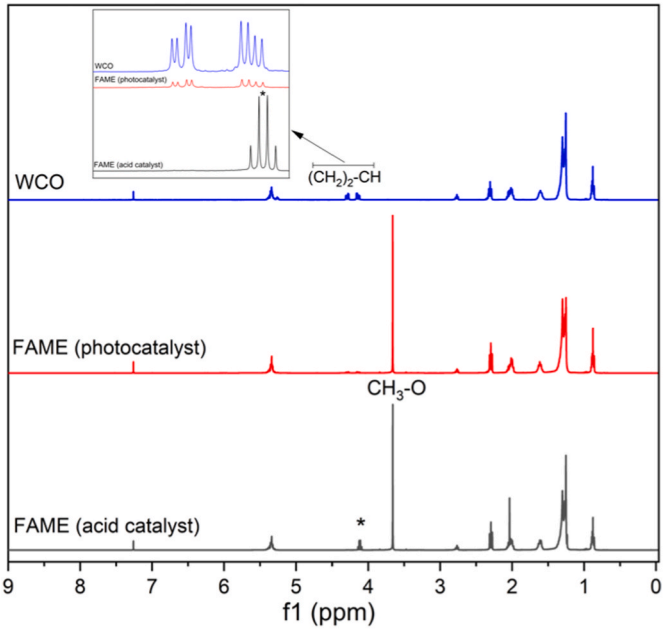


Fig. 4. ^{1}H NMR spectra (400 MHz, $CDCl_3$, 25 °C, chemical shift range 9.0–0.0 ppm) of crude WCO and FAME obtained by acid catalysis and TiO_2/UVA photocatalysis. The appearance of the methoxy proton signal of FAME (–OCH_3, ~3.6 ppm) confirms ester formation. Residual ethyl acetate is observed in the acid-catalysed sample, reflecting the solvent-based purification required in the homogeneous process (see Supplementary Section S5).

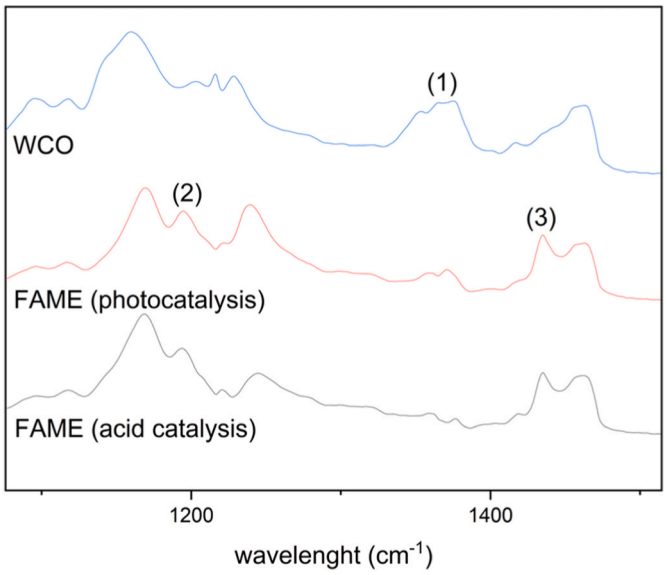


Fig. 5. FTIR–ATR spectra (Range: 100–1500 cm^{-1}) of crude WCO and FAME from simultaneous esterification and transesterification using acid catalysis and photocatalysis. Peaks: (1) 1375.5 cm^{-1} - aliphatic C-H (for CH_2 and CH_3), (2) 1196 cm^{-1} - O-CH_3 stretching, (3) 1434 cm^{-1} - CH_3 asymmetric bending (COO-CH_3) (Supplementary Material - Section S4).

as described in Section 3.5), causing the charge separation. As a consequence, electrons (e^-) are promoted to the conduction band (CB), resulting in positive holes (h^+) in the valence band (VB) [59]. The efficiency of this process depends on photon flux and charge-carrier lifetime, which directly influence the availability of reactive surface species. The methanol acesseses h^+ and generate the methoxy radical ($CH_3O^{\bullet}$), while e^- reacts with FFA or TGL, generating the corresponding carboxyl radical anion ($RCO_2^{-\bullet}H$ or $RCO_2^{-\bullet}R'$). Similar mechanisms were previously suggested for esterification [13,60,61] and transesterification [30] by TiO_2-photocatalysis. In the present system, both pathways occur simultaneously, where both, FFA and TGL, compete for the catalyst active sites. This step highlights the dual role of TiO_2 as both a photo-redox mediator and a surface that stabilises short-lived radical. Both radicals combine, generating FAME (biodiesel) via subsequent reaction steps. Radical recombination is facilitated at the catalyst surface, reducing the presence of side reactions or continued degradation, which contributes to the high selectivity observed for FAME formation.

The FFA pathway (esterification) generates FAME and water via a single-step reaction. The simpler reaction coordinate and smaller molecular size of FFAs favour faster surface interactions and lower energetic barriers for esterification. The TGL pathway (transesterification) occurs by three steps, where two intermediates are observed (DGL and MGL), and results in three molecules of FAME and one molecule of glycerol. These additional steps involve bulkier triglyceride species and sequential bond cleavage, making transesterification more sensitive to surface coverage, intermediate turnover, and mass-transfer limitations, consistent with its slightly lower conversion relative to esterification.

Moreover, the proposed photocatalytic mechanism of FAME production by both pathways (esterification and transesterification), is alligned with the kinetic data, mathematical modelling by appling the model F2B4, and the thermodynamic trends that will be discussed further in Section 3.6. The second-order dependence of the forward reaction is consistent with a bimolecular recombination between photoactivated methoxy species and acyl intermediates on the TiO_2 surface. In contrast, the apparent fourth-order dependence of the backward reaction reflects the involvement of multiple species and the system resistance.

3.4. Identification of byproducts from parallel reactions

Different byproducts may be produced in trace amounts, making their identification challenging. Methanol oxidation, for example, results in formaldehyde and subsequently formic acid (Fig. 7). Likewise, ester oxidation may generate a variety of compounds such as aldehydes, ketones, alkenes, and carboxylic acids [55,62]. Bak et al. [62] observed the presence of more than 30 compounds during thermal oxidation of methyl oleate and methyl palmitate oxidation. Temperatures above 380 °C resulted in larger amounts of 1-octane, 1-nonene, and methyl-5-hexenoate [62], which were not observed in FAME obtained by photocatalysis at lower temperatures. This contrast highlights a fundamental difference between thermal oxidation, where the bulk thermal energy is broadly applied and results in extensive chain scission reactions, and TiO_2-photocatalysis, where energy input is focused on specific regions of the chains, leading to the desired products.

In contrast, temperatures below 380 °C generated larger quantities of methyl acrylate, acetaldehyde, 2-decenal, 2-undecenal, and $C_{19}H_{36}O_3$ isomers [62]. Careful ^1H NMR analysis of FAME obtained by photocatalysis indicated the possible presence of the following compounds in trace amounts: methyl acrylate, acetaldehyde, butyraldehyde, 2-undecenal, and 2-decenal (Figs. 8 and 9). These were identified based on representative signals, whereas others could not be assigned due to their overlap with more dominant signals. The detection of these compounds is consistent with limited radical-mediated photooxidation pathways occurring in parallel with the main reaction, without leading to extensive ester degradation. It is important to note that FTIR-ATR and ^1H NMR spectroscopy provide qualitative rather than exhaustive or fully

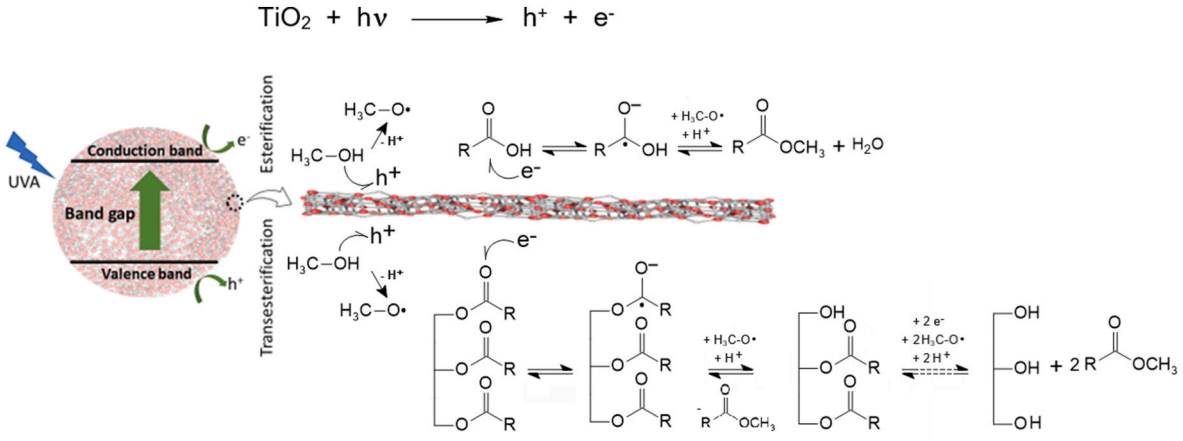


Fig. 6. Simultaneous esterification and transesterification of WCO with methanol photocatalysed by TiO_2.

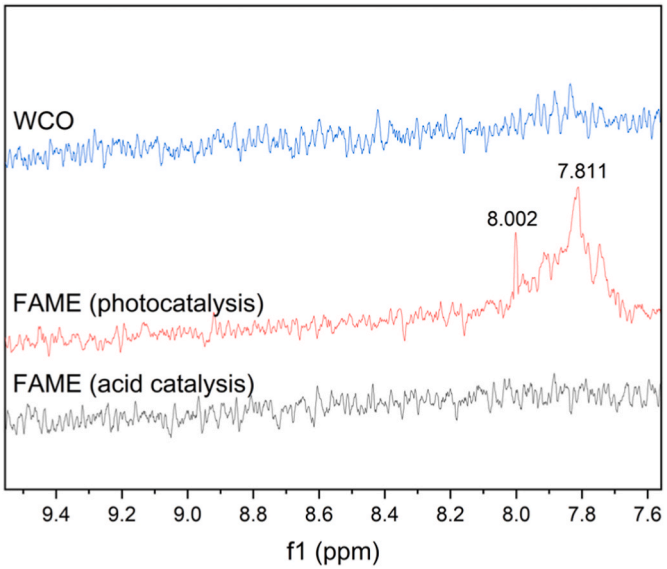


Fig. 7. Expanded ^{1}H NMR spectra (400 MHz, $CDCl_3$, 25 °C, 9.5–7.6 ppm) highlighting trace-level signals tentatively assigned to minor photooxidation byproducts, including formic acid (~8.00 ppm) and 2-(hydroxymethyl)acrylic acid (~7.81 ppm), originating from competing photooxidation reactions of esters. Signals are close to the detection limit and are interpreted qualitatively.

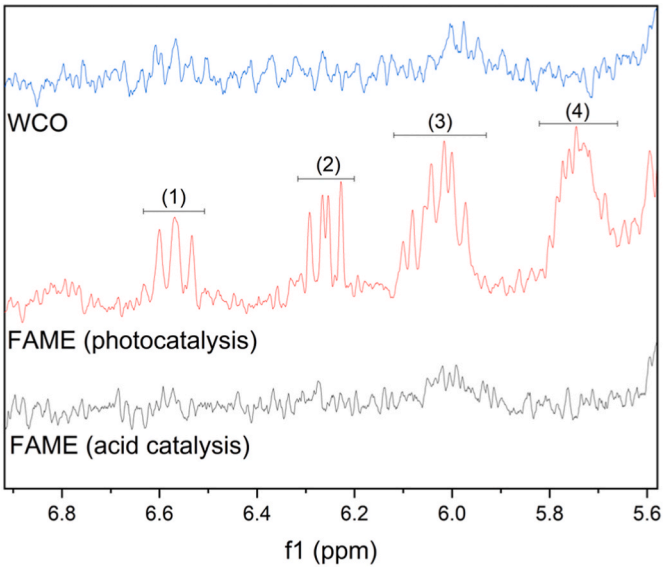


Fig. 9. Expanded ^{1}H NMR spectra (400 MHz, $CDCl_3$, 25 °C, 6.7–5.6 ppm) showing trace products from competing photooxidation reactions of esters. Peak assignments: (1) and (3, overlapping) olefinic protons of 2-decenal and 2-undecenal; (2), (3, overlapping), and (4) methyl acrylate and acrylic acid derivatives. Spectra are presented for qualitative comparison.

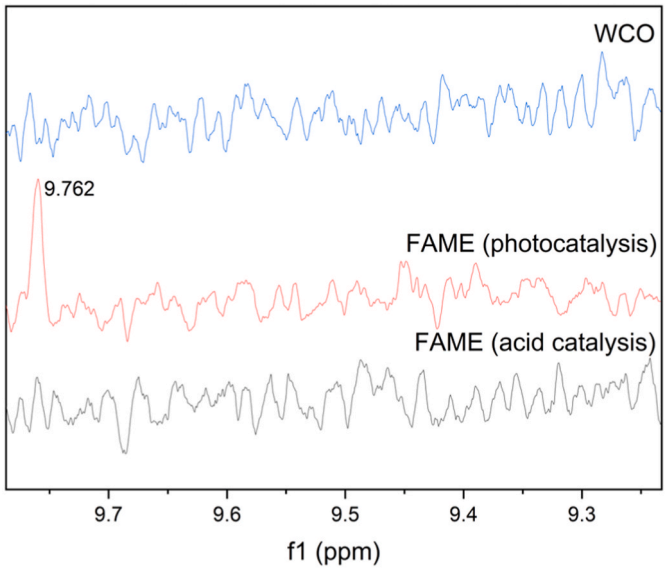


Fig. 8. Expanded ^{1}H NMR spectra (400 MHz, $CDCl_3$, 25 °C, 9.8–9.2 ppm) showing trace signals attributed to products of competing photooxidation reactions of esters, including methyl acrylate, acrylic acid, 2-decenal, and 2-undecenal (~9.76 ppm). The low signal-to-noise ratio reflects the minor formation of these species.

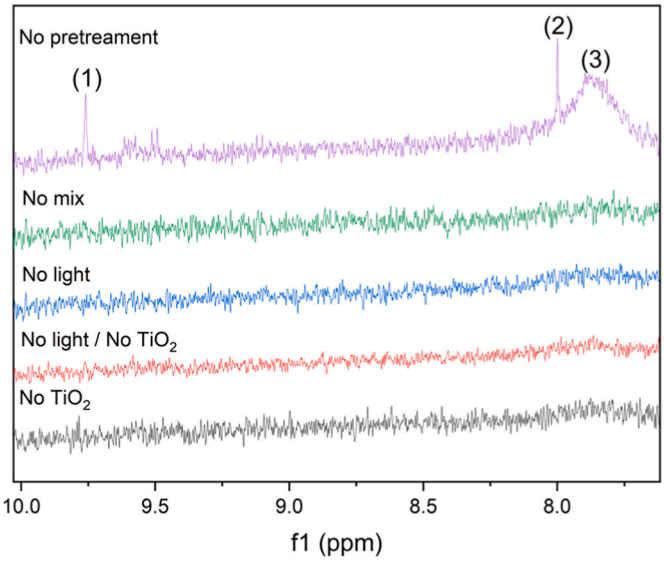


Fig. 10. Expanded ^{1}H NMR spectra (400 MHz, $CDCl_3$, 25 °C, 10.0–8.2 ppm) of blank experiments showing trace-level signals attributed to acetaldehyde, butyraldehyde, 2-decenal, and 2-undecenal (1), formic acid (2), and 2-(hydroxymethyl)acrylic acid (3). These species confirm the occurrence of minor background oxidation pathways under specific experimental conditions.

quantitative identification of reaction by-products, particularly when present at trace concentrations. While these techniques are effective for detecting characteristic functional groups and representative signals, they cannot fully exclude the presence of minor compounds below the detection or resolution limits. Therefore, both techniques were used in this study to identify indicative photooxidation products and assess their relative significance, rather than to claim the absolute absence of all possible byproducts.

The blank experiments (Figs. 10 and 11) revealed that the reaction performed without TiO_2 pretreatment followed the same parallel reactions as those observed during the regular photocatalytic reaction, however a low conversion was achieved (34%). The other blanks containing TiO_2 also showed traces of 2-decenal and 2-undecenal, even without light or under low FAME conversion (<34%) conditions. The blanks without TiO_2 did not result in any competing side reactions. This observation indicates that TiO_2 is required to initiate these minor pathways, but that their occurrence is not strongly dependent on photon flux or conversion level, suggesting a secondary, non-competitive nature. However, because these compounds were detected solely in trace concentrations, it was impossible to quantify or correlate these with the concentration of the main product (FAME). The absence of correlation between by-product formation and FAME yield further indicates that

these pathways do not significantly influence overall reaction kinetics or product selectivity. Consequently, these parallel pathways reactions were not included in the kinetic modelling, which focuses on the dominant esterification and transesterification reactions governing the system behaviour. Inclusion of trace by-products that neither accumulate nor influence the reaction rate would not improve model predictability and would compromise the physical relevance of the kinetic analysis. Moreover, FTIR-ATR and ^{1}H NMR spectroscopy provide qualitative rather than quantitative identification of reaction by-products, particularly when present at trace concentrations. While these techniques are effective for detecting characteristic functional groups and representative signals, they cannot fully exclude the presence of minor compounds below the detection or resolution limits. Therefore, both methods were used in this study to identify indicative photooxidation products and assess their relative significance, rather than to claim the absolute absence of all possible byproducts.

3.5. Catalyst characterisation

The catalyst (TiO_2) was qualitatively and quantitatively characterized before (TiO_2 pure), just after the photoreaction (0 RP), after the recovery process (1C) and at 5 cycles of reuse (5C). The mass loss of the catalyst was less than 1% and was neglected for further discussions. However, the physicochemical characteristics of the catalyst changed, as observed by FTIR-ATR, TGA and optical bandgap analysis, resulting in the decline of the catalytic activity upon reuse cycles. FTIR-ATR spectroscopy was performed to qualitatively identify the organic functional groups found on the TiO_2 surface. TGA/DSC profiles are interpreted as indicative of organic residue accumulation on the TiO_2 surface. The type of organic residue was determined by comparing the respective peaks of degradation/evaporation with the reactants and products pure compound degradation/evaporation peaks. The ratio between reactants and products was achieved based on relative mass-loss trends under thermal analysis over the reuse cycles.

These physicochemical analyses, when combined, indicate progressive accumulation of organic material on the TiO_2 surface. According to previous studies, as a consequence, aggregation phenomena occur over the cycles, whaich reduces the catalyst efectiveness []. The organic material content between 0RP (after the photoreaction) and 1C (after the recovery process) dropped by 77% (0RP: 39% and 1C: 9%), and the apparent bandgap decreased by 72% (0RP: 4.62 eV and 1C: 3.31 eV). These results indicate the efficiency of the recovery process by removing weakly adsorbed organic species, restoring light absorption, and partially recovering photocatalytic activity, as previously described for oleic acid [13].

However, the organic material mass gradually increased from 9 to 12% over the 5 cycles after the recovery process (1C to 5C), which results in an increase in the bandgap (3.31 eV to 3.59 eV). These results suggest that the organic material reduces access to the active sites and forms a film on the catalyst, limiting light penetration and the reaction efficiency as observed over the cycles [83% (1C) to 59% (5C)].

The FTIR-ATR spectroscopy (Fig. 12) qualitative analysis shows the presence of different organic compounds (reactants and products). The organic functional groups are found at C–H stretching bands (≈2920–2850 cm^{-1}) and carbonyl (C=O) vibrations (≈1740 cm^{-1}), consistent with adsorbed fatty acid methyl esters (FAME), residual triglycerides, and long-chain hydrocarbon species derived from WCO. By analysing the thermoanalysis (Fig. 13), the ratio between the degradation peaks indicates the highest content was observed for 0RP; however, all samples contained more WCO than FAME.

The preferential presence of WCO on the catalyst was caused by the naturally higher concentration of WCO at the beginning of the reaction, and the miscibility between biodiesel and methanol. The organic material retained on the catalyst consequently reduces light access, which increases the apparent bandgap of the catalyst [64] (Fig. 13 and Supplementary material – Section S7). This behaviour indicates that catalyst deactivation is dominated by surface fouling and optical shielding rather than structural degradation of TiO_2.

The combined effect of surface fouling and aggregation provides a mechanistic explanation for the observed reduction in conversion over successive reuse cycles. Evidence of surface fouling was inferred from the combined interpretation of FTIR-ATR, TGA/DSC mass-loss behaviour, and the systematic decline in catalytic activity upon reuse. Moreover, under the applied reaction conditions (≤65 °C), no evidence of catalyst sintering is expected, as these temperatures are far below those required for TiO_2 phase transformation or crystallite growth. Similarly, the observed behaviour is inconsistent with permanent loss of surface hydroxyl groups and is probably due to the progressive occupation of

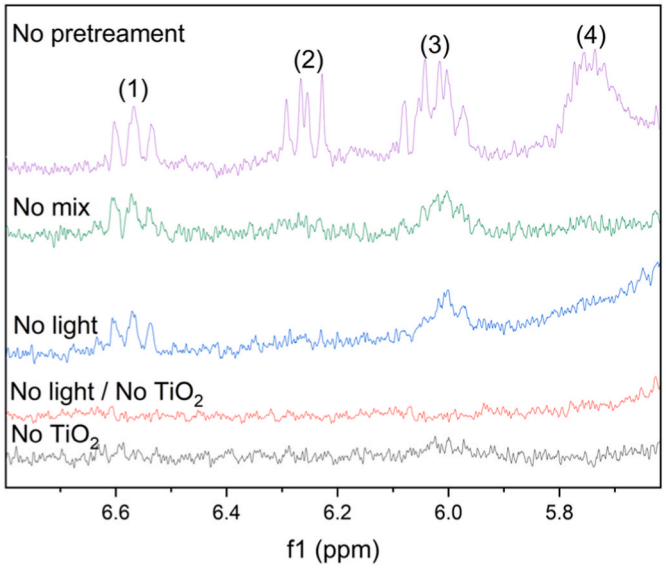


Fig. 11. Expanded ^{1}H NMR spectra (400 MHz, $CDCl_3$, 25 °C, 6.8–5.6 ppm) of blank experiments showing trace products from competing reactions of esters. Peak assignments follow those in Fig. 10, confirming that these species arise from parallel oxidation pathways rather than from productive esterification/transesterification reactions.

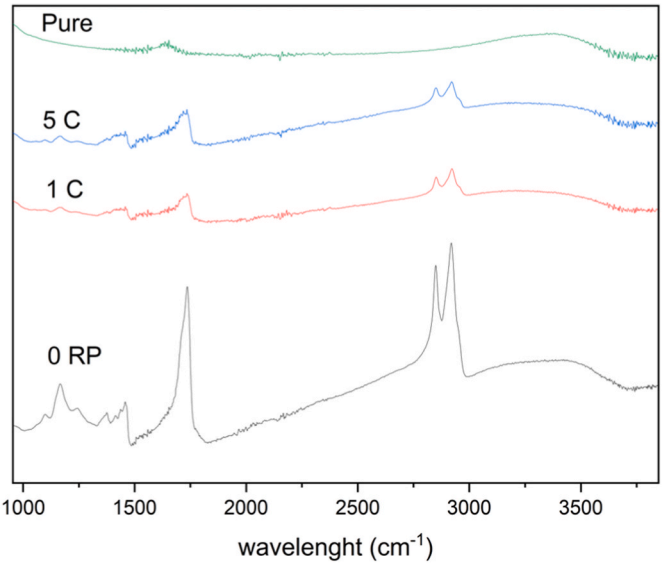


Fig. 12. ATR–FTIR spectra of the TiO_2 catalyst before reaction (pure), after photocatalysis without recovery (0RP), after one photocatalytic cycle with recovery (1C), and after five reuse cycles (5C). The progressive appearance of C–H and C=O bands indicates adsorption of organic species on the catalyst surface during repeated use.

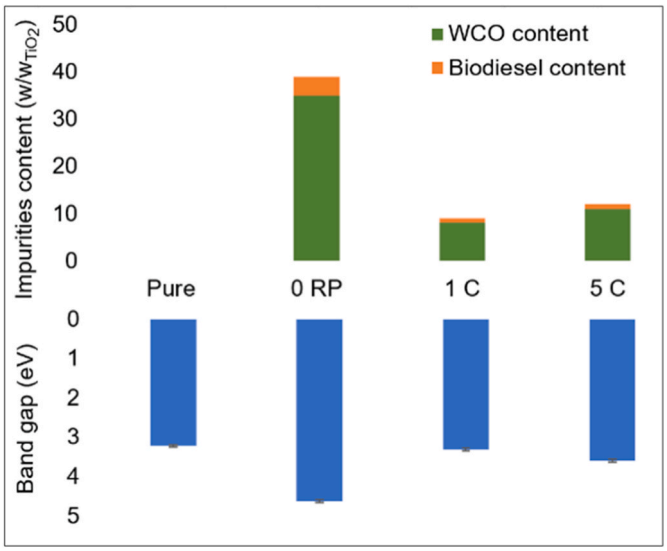


Fig. 13. UV–Vis diffuse reflectance spectra and corresponding Tauc plots used to estimate the apparent bandgap of TiO_2 before reaction (pure), after photocatalysis without recovery (0RP), after one recovy cycle (1C), and after five recovy cycles (5C). Variations in the apparent bandgap are attributed to surface fouling and light attenuation by adsorbed organic species rather than to structural modification of TiO_2. Estimated bandgap uncertainty is ±0.02 eV. The reference bandgap of pristine TiO_2 (P25 Evonik) is 3.18 eV [63].

surface sites by organic compounds. Moreover, the presence of organic residues promotes aggregation phenomena and reduces effective surface area and porosity, as reported in the literature [13,]. These effects further cause the mass and light-transfer resistance, what reinforces the cumulative nature of catalyst deactivation upon repeated reuse.

3.6. Kinetic modelling and thermodynamic properties

The plot of the kinetic curves of FAME ($C_{FAME}/C_{WCO,0}$) as a product of WCO and methanol TiO_2 photocatalysis under UVA irradiation was shown in Fig. 14. The graph shows the experimental and the mathematical modelling using the F2B4 model. Only this model is discussed at this stage. as it describes the experimental behaviour with higher statistical and thermodynamic accuracy. The equilibrium state was reached within three and 4 h for all experiments (UVA: 25-65 °C; Sunlight: 65 °C), so all the reactions were stopped after 4 h. Internal and external mass-transfer limitations were considered negligible under the experimental conditions applied. Thus, it was considered that the reaction rates were driven by surface photocatalytic kinetics rather than by transport phenomena. This assumption is supported by three main aspects.

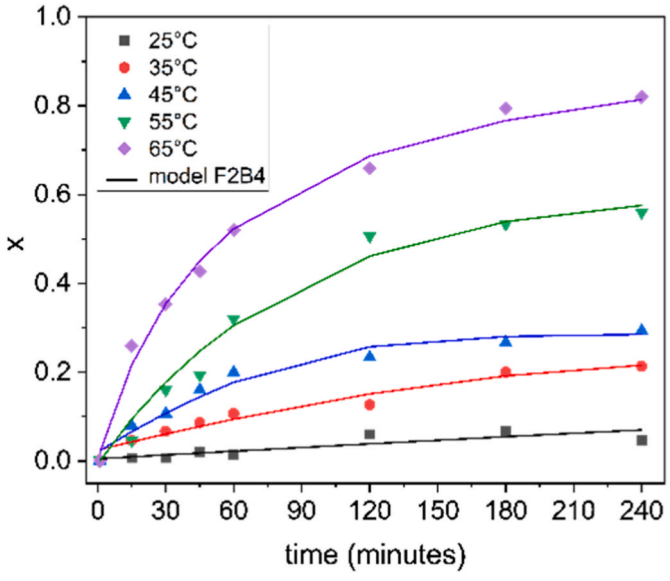


Fig. 14. Kinetic curves for simultaneous esterification and transesterification of WCO with methanol. Catalyst: TiO_2 irradiated with UVA or sunlight (1 WCO mol:55 MeOH mol, 20% TiO_2 w/w_{wco}).

(i) the use of vigorous agitation (500 rpm), which reduces drastically the mass transfer resistance. It is corroborate by the result obtained by the blank test in the absence of stirring, where only 25% conversion was achieved (Fig. 1).
(ii) a large excess of methanol leading to pseudo-homogeneous behaviour, as its initial and final concentration remains effectively constant.
(iii) the blank experiments demonstrated a strong dependence of conversion on light irradiation and catalyst presence rather than hydrodynamic conditions (details are given in Section 3.1).

In total, five models were applied (Table 1). Statistical analysis was conduted by evaluating the data from both curves, FAME increase, and WCO decrease. All the models converged with $R^2 > 0.90$ (Table 7), indicating that they statistically agree with the experimental results. However, beyond the statistically convergence, it is necessary to evaluate the parameters obtained by the respective models. In this case the kinetic and thermodynamic properties were determined (Table 8). However, only the model that considers the forward reaction as second-order and backward reaction as fourth-order (F2B4, $R^2 = 0.996$, Fig. 15) resulted in consistent parameter values in accordance with the literature.

Although TiO_2 is a heterogeneous photocatalyst, under the selected operating conditions (high stirring intensity and large methanol excess), the reacting medium behaves as a pseudo-homogeneous slurry at the reactor scale, such that bulk concentration profiles of WCO and FAME can be reasonably treated as spatially uniform. In this context, the homogeneous models (F1B1, F1B2, F2B2 and F2B4) are not intended to imply a truly homogeneous catalytic mechanism, but rather to provide phenomenological descriptions that allow discrimination of apparent reaction orders and reversibility trends from conversion–time data. The L–H model was included to explicitly account for adsorption-controlled surface kinetics and product inhibition, however this model did not describe the mechanism adequaly.

The thermodynamic parameters were obtained solely from the kinetic parameters obtained by the F2B4 model, after determining the rate constants which are a function of concentration (forward and backward reactions) and temperature. Subsequently, as described in Section 2.5; the Van't Hoff approach was applied. As a result, the enthalpy (ΔH), entropy (ΔS), and Gibbs free energy (ΔG) values should be interpreted as apparent thermodynamic parameters representative of the overall photocatalytic reaction system that guides to the reaction behavior, rather than as absolute thermodynamic properties of isolated elementary steps.

Table 7
Kinetic model statistical analysis applied to the predicted and experimental data for the simultaneous esterification and transesterification of WCO-methanol under photocatalysis.

Model	R^2	F-test	SD	β	t-student	p-value
F1B1	0.990	4726	0.021	0,995	68.745	0.000
F1B2	0.997	15361	0.012	0.999	123.939	0.000
F2B2	0.996	5279	0.014	0.984	72.656	0.000
F2B4	**0.996**	**4386**	**0.021**	**0.996**	**66.229**	**0.000**
L-H	0.995	25161	0.019	0.997	158.62	0.000

Table 8
Kinetic and thermodynamic parameters obtained from different mathematical models.

Model	k_{-1}[a]	k_1[a]	K^a_{eq}	$E_{a,B}$ (kJ/mol)	A_B	$E_{a,F}$ (kJ/mol)	A_F
F1B1	3.01E-03	1.34E-02	4.46E+00	−18 (R^2: 0.378)	6.14E-6 (R^2: 0.378)	63 (R^2: 0.963)	8.18E7 (R^2: 0.963)
F1B2	8.85E-03	1.24E-02	1.40E+00	−70 (R^2: 0.917)	8.12E+12 (R^2: 0.917)	44 (R^2: 0.886)	6.78E4 (R^2: 0.886)
F2B2	3.56E-10	4.66E-02	1.31E+08	68 (R^2: 0.973)	1.73E+9 (R^2: 0.973)	−289 (R^2: 0.525)	1.54E-51 (R^2: 0.525)
F2B4	1.73E+00	1.16E+01	6.68E+00	**224 (R^2: 0.791)**	**8.50E+15 (R^2: 0.791)**	**97 (R^2: 0.990)**	**2.87E+30 (R^2: 0.990)**
L-H	1.82E-03	1.16E+00	6.4E+02	−83 (R^2: 0.901)	1.41E15 (R^2: 0.901)	119 (R^2: 0.809)	1.15E+18 (R^2: 0.809)

[a] Temperature: 338.15 K.

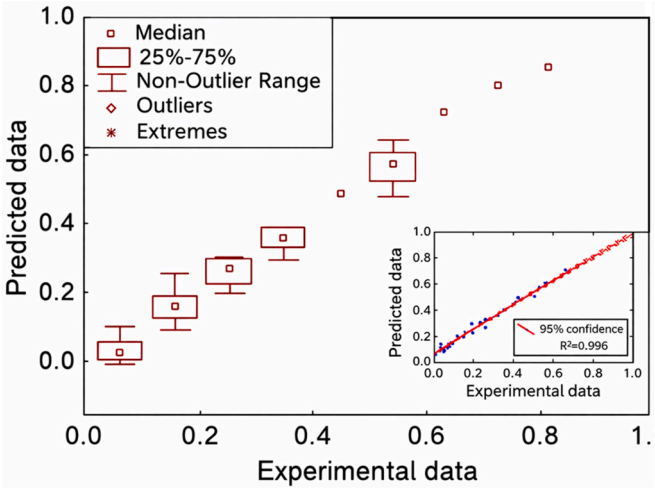


Fig. 15. Correlation between predicted (model F2B4) and experimental FAME conversion. □ 25%-75% = (−0.0089, 0.0078), I Non-Outlier (Range: −0.03 – 0.03), ■ Median = 0.0006, ● Outliers.

The values of activation energy ($Ea_{forward}$ of 97 kJ/mol and $Ea_{backward}$ of 224 kJ/mol) and the frequency of effective collisions between reacting molecules ($A_{forward}$ of 2.87E+30 and $A_{backward}$ of 8.50E+15) were determined by the Arrhenius equation considering the F2B4 kinetic model results. The substantially higher activation energy associated with the backward reaction, compared to the forward reaction, indicates that the reverse pathway is kinetically not feasible, particularly at lower temperatures, while the forward reaction is enhanced, as observed by the Arrhenius parameters (<E_a, and > A). The effective E_α, considering the entire process, was obtained applying Equation (8) and resulted in a linear decrease with increasing temperature (Fig. 16). It suggest that overall reaction kinetics under elevated-temperature photocatalytic conditions are preferable, as the E_α decreases. It indicates that the reaction becomes easier, what is consistent with the experimental data. This trend suggests that the system is energy-limited at lower temperatures (<45 °C). However, at higher temperatures (45 °C to 65 °C), the temperature barrier reduces and the reaction resistance becomes controlledy other factors, such as surface coverage, and/or product accumulation, for example.

The thermodynamic parameters are shown in Fig. 17. The values of ΔS (0.29 kJ/mol·K) and ΔH (92.58 kJ/mol) were obtained using the Van't Hoff model (Equation (9), Section 2.5). The equation requires the value of K_{eq} that was obtained by correlating the kinetic rates of the system. As the parameters were determined by the kinetic data experiments themselves, the thermodynamic parameters have to be considered specifically for this system and opertional conditions as a guide of the process physicochemical-thermodynamic response and behavior.

The positive value of enthalpy indicates the system requires energy to proceed and is therfore favoured at higher temperatures. The entropy is also positive, indicating that the molecular disorder tends to increase during the reaction. This increase in entropy can be attributed to the conversion of larger molecules, such as triglycerides and free fatty acids, into multiple ester molecules and glycerol. The formation of a greater number of molecular species, together with mixing and interfacial effects in the liquid-phase photocatalytic system, contributes to the overall increase in disorder.

The value of ΔG was determined by two different pathways. First, by correlating T and K_{eq} (Equation (10), ΔG1), and second, by correlating ΔH_R, T, and ΔS (Equation (11), ΔG2), respectively. However, both derivate from the same root, by considering the initial experimental kinetic data and matematical modelling (F2B4). Although, both approaches resulted in consistent values ($R^2 = 0.891$) and similar trends by

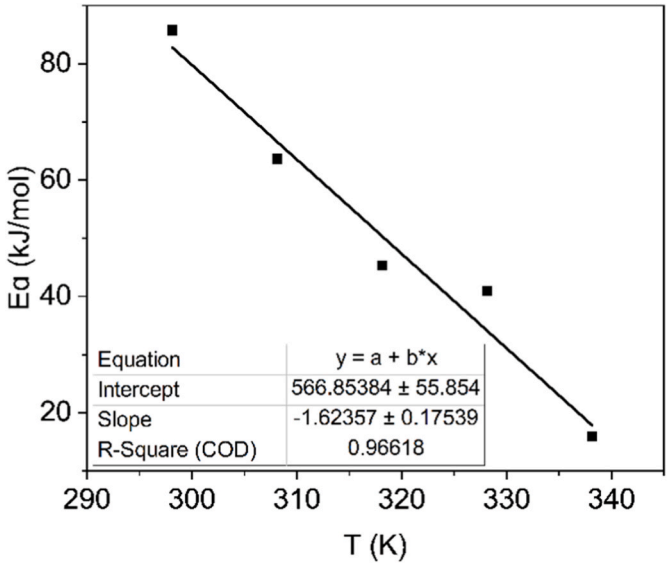


Fig. 16. Effective E_α of the reaction considering the F2B4 model.

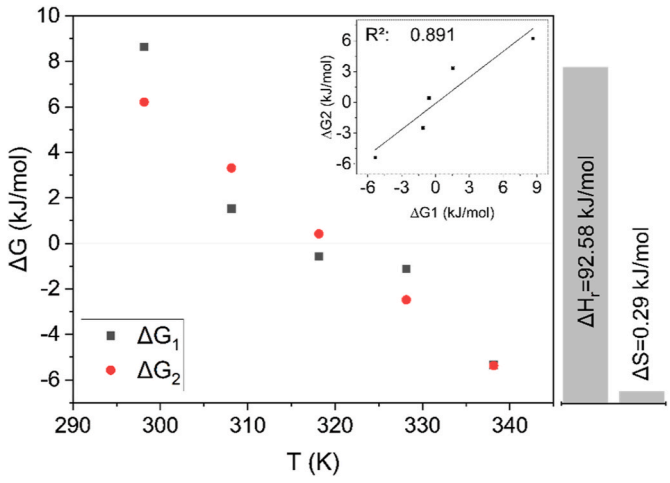


Fig. 17. Gibbs energy (ΔG), equilibrium constant (K_{eq}), Enthalpy (ΔH), and Entropy (ΔS) for simultaneous esterification and transesterification of WCO and methanol by TiO_2-photocatalysis with UVA-light (1 WCO mol:55MeOH mol, 20% TiO_2 w/w_{WCO}).

being positive at lower temperatures (<45 °C) and decreasing constantly as the temperature increases (45 °C to 65 °C). This trend is alligned with the previous discussion that indicates the endothermic nature of the reaction and the higher efficiency at higher temperatures.

By these specific thermodynamic parameters trend, it is possible to observe that as the temperature increases the TΔS term becomes more significant and gradually offsets the positive enthalpy. Around 45 °C, ΔG approaches zero, corresponding to the equilibrium region. Above this temperature, the entropy contribution becomes dominant, ΔG becomes negative, and the reaction becomes thermodynamically favourable, which explains the sharp increase in conversion observed experimentally. These results indicate an endothermic and effectively irreversible process between 45 and 65 °C under the studied operational conditions. Moreover, by increasing the temperature of the biphasic system, the miscibility between both reactants increases and consequently the mass-transfer resistance reduces, contributing to the faster covnersion.

4. Conclusion

Biodiesel was produced by TiO_2-photocatalysis from WCO and short-chain alcohols (methanol and ethanol) by simultaneous esterification and transesterification. Under the optimised operational conditions (1 mol WCO: 55 mol MeOH, 20% w/w_{wco} TiO_2, UVA irradiation, and 65 °C), a conversion of 83% (±1.24%) was achieved. Esterification resulted in a somewhat higher conversion (89%) than transesterification (81%), reflecting the different kinetic and mechanistic requirements of these parallel pathways under photocatalytic conditions. The developed process is thus suitable for producing biodiesel from feedstocks with high FFA content.

The catalyst was reusable, and even after five cycles, a reasonable conversion of 59% was achieved. Catalyst characterisation revealed the accumulation of organic material on the TiO_2 material, reducing the catalytic sites available and increasing the bandgap, and hence decreasing photocatalytic efficiency, highlighting surface fouling as the main factor limiting long-term photocatalytic performance.

Five different mathematical models were used to evaluate the experimental kinetic data. The model considering a second-order forward reaction and fourth-order backward reaction showed the best convergence with the predicted values (R^2: 0.996) and the kinetic and thermodynamic parameters. This demonstrates that statistical agreement alone is insufficient to describe the system, and that model discrimination based on physicochemical consistency is essential for interpreting photocatalytic biodiesel reactions. These parameters agreed with the observed behaviour, where the reaction was not efficient at temperatures below 45 °C, in accordance with the endothermic and entropy-driven nature of the process. The combined kinetic–thermodynamic analysis confirms that the low conversions observed at mild temperatures are not incidental, but arise from the intrinsically endothermic and entropy-driven nature of the photocatalytic system.

Simultaneous esterification and transesterification enables the use of high FFA contents overcoming a key limitation of conventional base-catalysed processes, which are commonly problematic in traditional thermal catalysts. Moreover, the use of heterogeneous photocatalysis can overcome many of the difficulties encountered using traditional homogeneous catalysts such as high temperature and extreme pH requirements, catalyst recovery and reuse challanges, low product purities that demand lenghty and resource-demanding purification steps, and specialized equipment needs due to the corrosive reaction conditions. Importantly, the photocatalytic route demonstrated high selectivity, with only trace amounts of side products detected, indicating controlled reaction pathways rather than extensive oxidative degradation.

While this study developed an efficient and eco-friendly process for the potential production of biodiesel, its main contribution lies in coupling photocatalytic experimentation with integrated kinetic and thermodynamic interpretation, more aspects need to be evaluated, such as optimising catalyst reuse, scale-up, implementation of different feedstocks, and natural sunlight utilization.

CRediT authorship contribution statement

Rosilene A. Welter: Writing – review & editing, Writing – original draft, Visualization, Validation, Methodology, Investigation, Formal analysis, Data curation, Conceptualization. **Harrson Santana:** Writing – review & editing, Supervision, Project administration. **Jayson Wau:** Methodology. **Osvaldir Pereira Taranto:** Supervision, Project administration. **Michael Oelgemöller:** Writing – review & editing, Supervision, Resources, Project administration.

Declaration of competing interest

The authors declare the following financial interests/personal relationships which may be considered as potential competing interests: Rosilene Andrea Welter Gabas reports financial support was provided by James Cook University. If there are other authors, they declare that they have no known competing financial interests or personal relationships that could have appeared to influence the work reported in this paper.

Acknowledgement

RAW wishes to thank the College of Science and Engineering at James Cook University for financial support (Competitive Research Training Grants 2021 and 2022). The authors thank Assoc.-Prof. George Vamvounis, and Dr. Shane Askew (James Cook University) for technical support.

Appendix A. Supplementary data

Supplementary data to this article can be found online at https://doi.org/10.1016/j.bmf.2026.100032.

Data availability

Data will be made available on request.

References

[1] Erin Voegele, NBB: Biodiesel can help meet USDA's AIA goals, biodiesel magazine. https://biodieselmagazine.com/articles/2517256/nbb-biodiesel-can-help-meet-usdaundefineds-aia-goals, 2020. (Accessed 23 January 2021).
[2] H. Esmaeili, A critical review on the economic aspects and life cycle assessment of biodiesel production using heterogeneous nanocatalysts, Fuel Process. Technol. 230 (2022) 107224, https://doi.org/10.1016/J.FUPROC.2022.107224.
[3] Oil World, Oil World (2022). https://www.oilworld.biz/. (Accessed 14 April 2022).
[4] G. Berrebi, P. Dufresne, Y. Jacquier, Recycling of spent hydroprocessing catalysts: EURECAT technology, Environ. Prog. 12 (1993) 97–100, https://doi.org/10.1016/0921-3449(94)90032-9.
[5] R. Ahmed, K. Huddersman, Review of biodiesel production by the esterification of wastewater containing fats oils and grease (FOGs), J. Ind. Eng. Chem. 110 (2022) 1–14, https://doi.org/10.1016/J.JIEC.2022.02.045.
[6] S. Maroa, F. Inambao, A review of sustainable biodiesel production using biomass derived heterogeneous catalysts, Eng. Life Sci. 21 (2021) 790, https://doi.org/10.1002/ELSC.202100025.
[7] O. Carp, C.L. Huisman, A. Reller, Photoinduced reactivity of titanium dioxide, Prog. Solid State Chem. 32 (2004) 33–177, https://doi.org/10.1016/J.PROGSOLIDSTCHEM.2004.08.001.
[8] K. Rajeshwar, M.E. Osugi, W. Chanmanee, C.R. Chenthamarakshan, M.V.B. Zanoni, P. Kajitvichyanukul, R. Krishnan-Ayer, Heterogeneous photocatalytic treatment of organic dyes in air and aqueous media, J. Photochem. Photobiol. C Photochem. Rev. 9 (2008) 171–192, https://doi.org/10.1016/J.JPHOTOCHEMREV.2008.09.001.
[9] I.K. Konstantinou, T.A. Albanis, Photocatalytic transformation of pesticides in aqueous titanium dioxide suspensions using artificial and solar light: intermediates and degradation pathways, Appl. Catal., B 42 (2003) 319–335, https://doi.org/10.1016/S0926-3373(02)00266-7.
[10] D. Kanakaraju, B.D. Glass, M. Oelgemöller, Titanium dioxide photocatalysis for pharmaceutical wastewater treatment, Environmetal Chemistry Letters 12 (2014) 27–47, https://doi.org/10.1007/s10311-013-0428-0.
[11] M.C. Manique, A.P. Silva, A.K. Alves, C.P. Bergmann, Application of hydrothermally produced TiO_2 nanotubes in photocatalytic esterification of oleic

acid, Mater. Sci. Eng., B 206 (2016) 17–21, https://doi.org/10.1016/J.MSEB.2016.01.001.
[12] R.A. Welter, H.S. Santana, L.G. de la Torre, M.C. Barnes, O.P. Taranto, M. Oelegemöller, Biodiesel production focusing on heterogenous catalysts and eco-friendly routes, ChemBioEng Rev. (2022).
[13] R.A. Welter, H. Santana, L.G. Torre, M. Robertson, O.P. Taranto, M. Oelgemöller, Methyl oleate synthesis by TiO_2 photocatalytic esterification of oleic acid: optimisation by response surface quadratic methodology, reaction kinetics and thermodynamics, ChemPhotoChem 6 (2022) e202200007, https://doi.org/10.1002/cptc.202200007.
[14] N.G. Khaligh, T. Mihankhah, Z. Shahnavaz, L. Zaharani, M.R. Johan, Solar energy and TiO2 nanotubes: biodiesel production from waste cooking olive oil, Environ. Prog. Sustain. Energy 40 (2021), https://doi.org/10.1002/ep.13537.
[15] M. Khan, H. Farah, N. Iqbal, T. Noor, M.Z. Bin Amjad, S.S. Ejaz Bukhari, A TiO_2 composite with graphitic carbon nitride as a photocatalyst for biodiesel production from waste cooking oil, RSC Adv. 11 (2021) 37575–37583, https://doi.org/10.1039/D1RA07796A.
[16] V. Domínguez-Barroso, C. Herrera, M.Á. Larrubia, C. Gonzalo López, D.B. Ramos, L.J. Alemany, Heterogeneization of biodiesel production by simultaneous esterification and transesterification of oleins, Catalysts 14 (2024) 871, https://doi.org/10.3390/CATAL14120871, 14 (2024) 871.
[17] N.M. Alahmar, N.I.B.W. Azelee, S. Toemen, Efficient biodiesel production from waste cooking oil using a bifunctional Ce/Mn/γ-Al_2O_3 catalysts, Sci. Rep. 15 (2025) 352, https://doi.org/10.1038/s41598-024-82845-2, 2024 15:1.
[18] S.M. Farouk, A.M. Tayeb, S.M.S. Abdel-Hamid, R.M. Osman, Recent advances in transesterification for sustainable biodiesel production, challenges, and prospects: a comprehensive review, Environ. Sci. Pollut. Control Ser. 31 (2024) 12722–12747, https://doi.org/10.1007/S11356-024-32027-4, 2024 31:9.
[19] V.S. Shanthini, D. Chitra, G. Moorthy, Biodiesel: a comprehensive review of properties, catalyst types, and feedstock sources, Results Chem. 18 (2025) 102678, https://doi.org/10.1016/J.RECHEM.2025.102678.
[20] M. Yue, S.L. Rokhum, X. Ma, T. Wang, H. Li, Z. Zhao, Y. Wang, H. Li, Recent advances of biodiesel production enhanced by external field via heterogeneous catalytic transesterification system, Chem. Eng. Process. Process Intensif. 205 (2024) 109997, https://doi.org/10.1016/J.CEP.2024.109997.
[21] K. Brindhadevi, P.T. Kim, A. Chinnathambi, S.K. Kamarudin, A. Pugazhendhi, Comparison of photocatalytic vs conventional transesterification for biodiesel preparation from fish waste oil using green TiO2/SiO2 catalyst, Process Saf. Environ. Prot. 188 (2024) 167–176, https://doi.org/10.1016/J.PSEP.2024.05.039.
[22] C.Y. Lin, S.L. Tseng, Influence of solid alkaline photocatalysts irradiated with UV light on fuel properties of palm oil biodiesel, ACS Omega (2024), https://doi.org/10.1021/ACSOMEGA.4C04991.
[23] A.N. Abdulkareem, N.F. Nasir, A comprehensive review of biodiesel production using heterogeneous catalyst, Journal of Advanced Research in Micro and Nano Engineering 22 (2024) 103–115, https://doi.org/10.37934/ARMNE.22.1.103115.
[24] M.V.D. Silva, C.E. Hori, M.H.M. Reis, Thermochemical data of the oleic acid esterification reaction: a quantum mechanics approach, Fluid Phase Equilib. 406 (2015) 168–174, https://doi.org/10.1016/j.fluid.2015.07.050.
[25] ARPANSA, Australian radiation protection and nuclear safety agency. https://www.arpansa.gov.au/our-services/monitoring/ultraviolet-radiation-monitoring/ultraviolet-radiation-index, 2022 (accessed January 10, 2022).
[26] J. Tauc, R. Grigorovici, A. Vancu, Optical properties and electronic structure of amorphous germanium, Phys. Status Solidi 15 (1966) 627–637, https://doi.org/10.1002/pssb.19660150224.
[27] P. Makuła, M. Pacia, W. Macyk, How to correctly determine the band gap energy of modified semiconductor photocatalysts based on UV–Vis spectra, J. Phys. Chem. Lett. 9 (2018) 6814–6817, https://doi.org/10.1021/acs.jpclett.8b02892.
[28] J.D. McCurry, GC Analysis of Total Fatty Acid Methyl Esters (FAME) and Methyl Linolenate in Biodiesel Using the Revised EN14103:2011 Method, 2012.
[29] G. Gelbard, O. Brès, R.M. Vargas, R. Vielfaure, U.F. Schuchardt, ^{1}H nuclear Magnetic resonance determination of the yield of the transesterification of rapessed oil with methanol, J. Am. Oil Chem. Soc. 72 (1995) 1239–1241, https://doi.org/10.1007/BF02540998.
[30] M.J. Borah, A. Devi, R.A. Saikia, Dhanapati deka, biodiesel production from waste cooking oil catalyzed by in-situ decorated TiO2 on reduced graphene oxide nanocomposite, Energy 158 (2018) 881–889.
[31] S.K. Jaiswal, N. Tejo Prakash, R. Prakash, ^{1}H NMR based quantification of ethyl ester in biodiesel: a comparative study of product-dependent derivations, Analytical Chemistry Letters 6 (2016) 518–525, https://doi.org/10.1080/22297928.2016.1246977.
[32] A. Abdelkhalik, H. Elsayed, M. Hassan, M. Nour, A.B. Shehata, M. Helmy, Using thermal analysis techniques for identifying the flash point temperatures of some lubricant and base oils, Egypt. J. Pet. 27 (2018) 131–136, https://doi.org/10.1016/J.EJPE.2017.02.006.
[33] J.J. Lu, W.H. Chen, Investigation on the ignition and burnout temperatures of bamboo and sugarcane bagasse by thermogravimetric analysis, Appl. Energy 160 (2015) 49–57, https://doi.org/10.1016/J.APENERGY.2015.09.026.
[34] N. Khan, S.H. Park, L. Kadima, C. Bourdeau, E. Calina, C.W. Edmunds, D.P. Pursell, Locally sustainable biodiesel production from waste cooking oil and grease using a deep eutectic solvent: characterization, thermal properties, and blend performance, ACS Omega 6 (2021) 9204–9212, https://doi.org/10.1021/acsomega.1c00556.
[35] J. Wnorowska, S. Ciukaj, S. Kalisz, Thermogravimetric analysis of solid biofuels with additive under air atmosphere, Energies 14 (2021) 2257, https://doi.org/10.3390/en14082257.
[36] Y. Lai, B. Wang, X. Chen, Y. Yuan, L. Zhong, X. Qiao, Y. Zhang, M. Yuan, J. Shu, P. Wang, Thermogravimetric analysis of combustion characteristics of palm oil and rapeseed oil biodiesel, Biotechnology 14 (2014) 9–15, https://doi.org/10.3923/biotech.2015.9.15.
[37] T. Liavitskaya, S. Vyazovkin, Discovering the kinetics of thermal decomposition during continuous cooling, Phys. Chem. Chem. Phys. 18 (2016) 32021–32030, https://doi.org/10.1039/C6CP04507C.
[38] N. Sbirrazzuoli, Interpretation and physical meaning of kinetic parameters obtained from isoconversional kinetic analysis of polymers, Polymers 12 (2020) 1280, https://doi.org/10.3390/polym12061280.
[39] A. Al-Saadi, B. Mathan, Y. He, Biodiesel production via simultaneous transesterification and esterification reactions over SrO–ZnO/Al_2O_3 as a bifunctional catalyst using high acidic waste cooking oil, Chem. Eng. Res. Des. 162 (2020) 238–248, https://doi.org/10.1016/j.cherd.2020.08.018.
[40] M. Guo, W. Jiang, J. Ding, J. Lu, Highly active and recyclable CuO/ZnO as photocatalyst for transesterification of waste cooking oil to biodiesel and the kinetics, Fuel 315 (2022) 123254, https://doi.org/10.1016/j.fuel.2022.123254.
[41] A. De, S.S. Boxi, Application of Cu impregnated TiO2 as a heterogeneous nanocatalyst for the production of biodiesel from palm oil, Fuel 265 (2020) 117019, https://doi.org/10.1016/J.FUEL.2020.117019.
[42] T. Mihankhah, M. Delnavaz, N.G. Khaligh, Application of TiO2 nanoparticles for eco-friendly biodiesel production from waste olive oil, Int. J. Green Energy 15 (2018) 69–75, https://doi.org/10.1080/15435075.2018.1423975.
[43] Z. Wen, X. Yu, S.T. Tu, J. Yan, E. Dahlquist, Biodiesel production from waste cooking oil catalyzed by TiO2–MgO mixed oxides, Bioresour. Technol. 101 (2010) 9570–9576, https://doi.org/10.1016/J.BIORTECH.2010.07.066.
[44] S.A. Hawash, E.E. Ebrahiem, H.A. Farag, Kinetic study of the esterification of unsaturated free fatty acids, Proceedings of the Institution of Civil Engineers - Energy 172 (2019) 105–114, https://doi.org/10.1680/jener.19.00006.
[45] D. Kanakaraju, C.A. Motti, B.D. Glass, M. Oelgemöller, Solar photolysis versus TiO_2-mediated solar photocatalysis: a kinetic study of the degradation of naproxen and diclofenac in various water matrices, Environ. Sci. Pollut. Control Ser. 23 (2016) 17437–17448, https://doi.org/10.1007/s11356-016-6906-8.
[46] M. Oelgemöller, Solar photochemical synthesis: from the beginnings of organic photochemistry to the solar manufacturing of commodity chemicals, Chem. Rev. 116 (2016) 9664–9682, https://doi.org/10.1021/acs.chemrev.5b00720.
[47] L. Liu, Z. Liu, G. Tang, W. Tan, Esterification of Free Fatty Acids in Waste Cooking Oil by Heterogeneous Catalysts, vol. 20, Transactions of Tianjin University, 2014, pp. 266–272, https://doi.org/10.1007/s12209-014-2242-6.
[48] M. Hassani, G. Amini, G. Najafpour, S.M. Rabiee, A two-step catalytic production of biodiesel from waste cooking oil, Int. J. Eng. 26 (2013) 563–570, https://doi.org/10.5829/idosi.ije.2013.26.06c.01.
[49] K.A. Shah, J.K. Parikh, K.C. Maheria, Optimization studies and chemical kinetics of silica Sulfuric acid-catalyzed biodiesel synthesis from waste cooking oil, Bioenergy Res. 7 (2014) 206–216, https://doi.org/10.1007/s12155-013-9363-y.
[50] J. Salimon, A.A. Ishak, Optimization process for esterification of rubber seed oil (RSO) with trimethylolpropane (TMP), J. Sci. Technol. 4 (2012) 81–90.
[51] V.M. Abbasov, H.M. Abd El-Lateef, L.I. Aliyeva, E.E. Qasimov, I.T. Ismayilov, M. M. Khalaf, A study of the corrosion inhibition of mild steel C1018 in CO2-saturated brine using some novel surfactants based on corn oil, Egypt. J. Pet. 22 (2013) 451–470, https://doi.org/10.1016/J.EJPE.2013.11.002.
[52] J. Gardy, A. Hassanpour, X. Lai, M.H. Ahmed, M. Rehan, Biodiesel production from used cooking oil using a novel surface functionalised TiO2 nano-catalyst, Appl. Catal., B 207 (2017) 297–310, https://doi.org/10.1016/J.APCATB.2017.01.080.
[53] S.S.M. Mostafa, N.S. El-Gendy, Evaluation of fuel properties for microalgae Spirulina platensis bio-diesel and its blends with Egyptian petro-diesel, Arab. J. Chem. 10 (2017) S2040–S2050, https://doi.org/10.1016/J.ARABJC.2013.07.034.
[54] R.M. Smith, A.E. Martell, NIST Critically Selected Stability Constants of Methal Complexes Database, vol. 46, NIST Standard Reference Database, 2004.
[55] C.v. Naik, C.K. Westbrook, O. Herbinet, W.J. Pitz, M. Mehl, Detailed chemical kinetic reaction mechanism for biodiesel components methyl stearate and methyl oleate, Proc. Combust. Inst. 33 (2011) 383–389, https://doi.org/10.1016/J.PROCI.2010.05.007.
[56] V. Pugnet, S. Maury, V. Coupard, A. Dandeu, A.A. Quoineaud, J.L. Bonneau, D. Tichit, Stability, activity and selectivity study of a zinc aluminate heterogeneous catalyst for the transesterification of vegetable oil in batch reactor, Appl. Catal. Gen. 374 (2010) 71–78, https://doi.org/10.1016/J.APCATA.2009.11.028.
[57] H. Noureddini, D. Zhu, Kinetics of transesterification of soybean oil, J. Am. Oil Chem. Soc. 74 (1997) 1457–1463, https://doi.org/10.1007/s11746-997-0254-2.
[58] X. Chen, Z. Li, Y. Chun, F. Yang, H. Xu, X. Wu, Effect of the formation of diglycerides/monoglycerides on the kinetic curve in oil transesterification with methanol catalyzed by calcium oxide, ACS Omega 5 (2020) 4646–4656, https://doi.org/10.1021/acsomega.9b04431.

[59] B. Ohtani, Photocatalysis by inorganic solid materials: revisiting its definition, concepts, and experimental procedures, Adv. Inorg. Chem. 63 (2011) 395–430, https://doi.org/10.1016/B978-0-12-385904-4.00001-9.
[60] M. Guo, W. Jiang, C. Chen, S. Qu, J. Lu, W. Yi, J. Ding, Process optimization of biodiesel production from waste cooking oil by esterification of free fatty acids using La^{3+}/ZnO-TiO_2 photocatalyst, Energy Convers. Manag. 229 (2021) 113745, https://doi.org/10.1016/J.ENCONMAN.2020.113745.
[61] N. Ghani, J. Iqbal, S. Sadaf, H.N. Bhatti, M. Asgher, Comparison of photo-esterification capability of bismuth vanadate with reduced graphene oxide bismuth vanadate (RGO/$BiVO_4$) composite for biodiesel production from high free fatty acid containing non-edible oil, ChemistrySelect 5 (2020) 9245–9253, https://doi.org/10.1002/SLCT.202001913.
[62] S. Bax, M.H. Hakka, P.-A. Glaude, O. Herbinet, F. Battin-Leclerc, Experimental study of the oxidation of methyl oleate in a jet-stirred reactor, Combust. Flame 157 (2010) 1220–1229, https://doi.org/10.1016/j.combustflame.2009.12.008.
[63] T. Ishigaki, Y. Nakada, N. Tarutani, T. Uchikoshi, Y. Tsujimoto, M. Isobe, H. Ogata, C. Zhang, D. Hao, Enhanced visible-light photocatalytic activity of anatase-rutile mixed-phase nano-size powder given by high-temperature heat treatment, R. Soc. Open Sci. 7 (2020) 191539, https://doi.org/10.1098/rsos.191539.
[64] T. Luttrell, S. Halpegamage, J. Tao, A. Kramer, E. Sutter, M. Batzill, Why is anatase a better photocatalyst than rutile? - model studies on epitaxial TiO2 films, Sci. Rep. 4 (2015) 4043, https://doi.org/10.1038/srep04043.